Stem Cell Reports
Resource
ISSCR
OPEN ACCESS

Recapitulation of Human Neural Microenvironment Signatures in iPSC-Derived NPC 3D Differentiation

Daniel Simão,[1,2] Marta M. Silva,[1,2] Ana P. Terrasso,[1,2] Francisca Arez,[1,2] Marcos F.Q. Sousa,[1,2] Narges Z. Mehrjardi,[3] Tomo Šarić,[3] Patrícia Gomes-Alves,[1,2] Nuno Raimundo,[4] Paula M. Alves,[1,2] and Catarina Brito[1,2,*]

[1]iBET, Instituto de Biologia Experimental e Biológica, Oeiras, Portugal
[2]Instituto de Tecnologia Química e Biológica António Xavier, Universidade Nova de Lisboa, Oeiras, Portugal
[3]Center for Physiology and Pathophysiology, Institute for Neurophysiology, Medical Faculty, University of Cologne, Cologne 50931, Germany
[4]Universitätsmedizin Göttingen, Institut für Zellbiochemie, Göttingen, Germany
*Correspondence: anabrito@ibet.pt
https://doi.org/10.1016/j.stemcr.2018.06.020

SUMMARY

Brain microenvironment plays an important role in neurodevelopment and pathology, where the extracellular matrix (ECM) and soluble factors modulate multiple cellular processes. Neural cell culture typically relies on heterologous matrices poorly resembling brain ECM. Here, we employed neurospheroids to address microenvironment remodeling during neural differentiation of human stem cells, without the confounding effects of exogenous matrices. Proteome and transcriptome dynamics revealed significant changes at cell membrane and ECM during 3D differentiation, diverging significantly from the 2D differentiation. Structural proteoglycans typical of brain ECM were enriched during 3D differentiation, in contrast to basement membrane constituents in 2D. Moreover, higher expression of synaptic and ion transport machinery was observed in 3D cultures, suggesting higher neuronal maturation in neurospheroids. This work demonstrates that 3D neural differentiation as neurospheroids promotes the expression of cellular and extracellular features found in neural tissue, highlighting its value to address molecular defects in cell-ECM interactions associated with neurological disorders.

INTRODUCTION

CNS development culminates in the establishment of highly specialized structures, where the architectural and biochemical features of the extracellular space play a pivotal role in maintaining tissue function. Neurons, glia, and other non-neural cells (e.g., endothelial cells) contribute to this microenvironment through the secretion/uptake of extracellular matrix (ECM) components and soluble factors. ECM composition undergoes an intense remodeling process during CNS development, which is essential to support cell migration and promote axonal growth/guidance and synaptogenesis (Bandtlow and Zimmermann, 2000).

Neural ECM differs in composition from other tissues, containing low levels of basement membrane constituents such as collagen, laminin, and fibronectin (Rutka et al., 1988). Instead, the neural ECM is highly enriched in proteoglycans (PGs), including chondroitin sulfate PGs (CSPGs) and heparan sulfate PGs (HSPGs), link proteins (e.g., tenascin-R and tenascin-C) and hyaluronic acid (Soleman et al., 2013). Lecticans are the most important family of CSPGs found in brain tissue, namely the ubiquitously expressed aggrecan and versican and the CNS-specific brevican and neurocan (Howell and Gottschall, 2012). In the final stages of neuronal development these CSPGs accumulate around somatic and dendritic synapses, generating the cartilage-like structures perineuronal nets (PNNs) (Wang and Fawcett, 2012). PNN formation plays a major role in retaining the existing synaptic network and regulating synaptic plasticity. This has been demonstrated by enzymatic digestion of CSPGs, which results in impairment of long-term potentiation/depression and changes the neuronal network activity toward more naive patterns (Bikbaev et al., 2015). Perturbations in neural microenvironment homeostasis have been also associated with pathological events in several neurological disorders, both at a causal or modulatory level. Many studies have suggested a link between ECM alterations and brain injuries (e.g. traumatic brain injury, stroke) (Kim et al., 2016) or Alzheimer's disease (Snow et al., 1994).

Despite increasing evidence linking alterations of neural microenvironment with neurological pathologies, the availability and validity of *in vitro* models to address these questions remains uncertain. Organotypical cultures are considered the most accurate model available, preserving ECM composition and tissue architecture. Nevertheless challenges arise from the use of these cultures, namely the scarcity of human tissue, the difficulty in maintaining long-term cultures, and ensuring optimal culture conditions to attain a model that represents a non-inflamed and non-reactive tissue (Humpel, 2015). The use of human induced pluripotent stem cells (hiPSCs) provides a stable and renewable source of human neural cells, also providing access to patient-derived cells with the disease-associated genetic background. Moreover, the combination of hiPSC

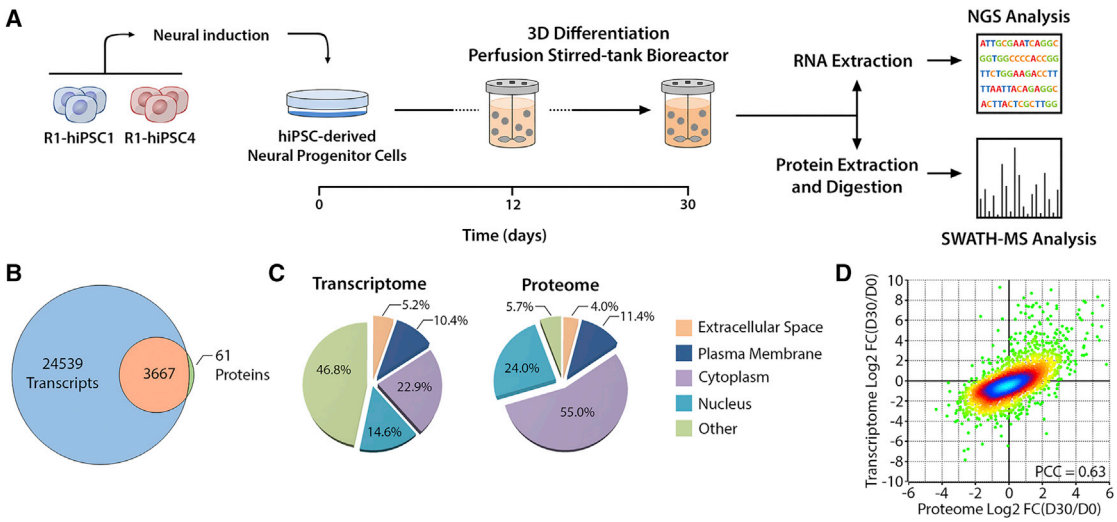

Figure 1. Schematic Workflow for hiPSC-Derived NPC 3D Differentiation

(A) NPCs were derived from two hiPSC lines, expanded as monolayer, and differentiated as neurospheroids. Cells harvested at days 0, 12, and 30 were processed for transcriptomic or proteomic analysis.

(B) The coverage and overlap between total identified transcripts and proteins are represented in the Venn diagram.

(C) Cellular localization of the identified transcripts and proteins according to Ingenuity Pathway Analysis (IPA) knowledge base.

(D) Density scatterplot describes the transcriptome-proteome correlation, where each dot indicates the fold change (logarithmized) of an individual transcript/protein (total of 3,667). The Pearson correlation coefficient (PCC) is indicated in the scatterplot. The color code represents the density of dots included in a region of the scatterplot. Data shown represent four pooled independent biological experiments (two independent experiments of two cell lines).

See also Figures S1 and S2.

with three-dimensional (3D) culture systems supports the development of more accurate *in vitro* cell models, relative to traditional two-dimensional (2D) monolayer systems. Human stem cell-derived 3D *in vitro* neural models have been shown to recapitulate important features of the target tissue, namely neuron-glia interactions (Simão et al., 2016a) or cellular organization (Lancaster and Knoblich, 2014; Lancaster et al., 2013). However, most of these rely on the use of exogenous matrices, and their ability to mimic neural extracellular space features remains elusive. We hypothesized that 3D differentiation of hiPSC-derived human neural progenitor cells (hNPCs) as neurospheroids, in perfusion stirred-tank bioreactors, could sustain a microenvironment remodeling toward ECM components typical of neural ECM. To address this question, we applied transcriptome sequencing and quantitative proteomics during 3D *in vitro* differentiation. Here we demonstrate that 3D differentiation as neurospheroids promotes the secretion and accumulation of neural ECM structural components and expression of synaptic machinery, typically found in neural tissue. This study demonstrates that human stem cell-derived 3D neural models are promising tools to address the role of neural microenvironment in healthy and diseased states and are potential tools for the development of novel therapeutic strategies targeting neural ECM.

RESULTS

Transcriptomic and Proteomic Analysis of hiPSC-NPC 3D Differentiation

Two NPC lines derived from hiPSCs (Figure S1) were used to address the molecular remodeling process occurring during 3D differentiation, at both transcriptomic and proteomic levels (Figures 1A and S2). We used a 3D culture strategy previously established by our group (Simão et al., 2016b) to generate and differentiate neurospheroids. Three representative time points were selected for analysis, including an initial sampling from the hiPSC-NPC cultures used for inoculation of 3D cultures (day 0), an early differentiation state (day 12), and a late differentiation state (day 30). The initial 7 days of culture correspond to a cell aggregation stage performed in presence of epidermal growth factor and basic fibroblast growth factor. This step promotes self-assembly of cells into compact neurospheres (~100 μm diameter; Figures S1L and S1M) while maintaining a proliferative phenotype, as demonstrated by the incorporation of 5-ethynyl-2′-deoxyuridine (EdU) in approximately 65% of cells (Figure S1O). Still, the cell density remained almost constant, around 5×10^5 cells/mL (Figure S1N), indicating a considerable decrease of cell growth rate in the 3D cultures. Along differentiation, a drastic decrease in the

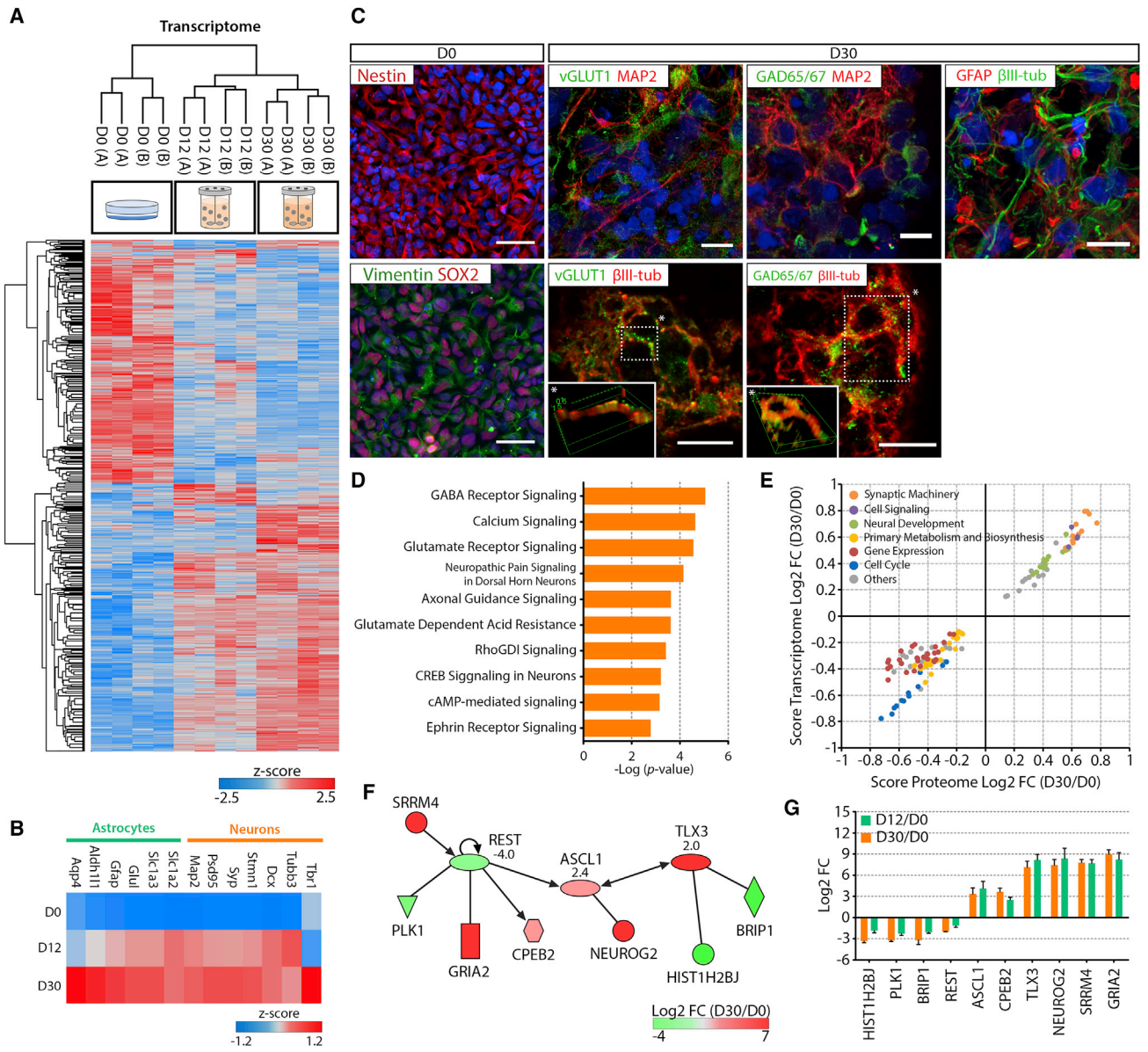

Figure 2. Transcriptome Dynamics during hiPSC-NPC 3D Differentiation

(A) Heatmap of significantly modulated transcripts between days 0 (D0), 12 (D12), and 30 (D30) (total of 12,116). Hierarchical clustering performed for the biological replicates of each time point and cell line (in columns; A and B refer to R1-hiPSC1-NPC and R1-hiPSC4-NPC, respectively), and for transcripts (in rows). Significantly modulated transcripts identified by multi-sample ANOVA test with a permutation-based false discovery rate (FDR) cutoff of 0.05 applied on the logarithmized intensities. *Z*-score values were color coded from blue (downregulation) to red (upregulation).

(B) Heatmaps of gene expression profiles of neuronal and astrocytic specific markers at day D0, D12, and D30. *Z* score values were color coded from blue (downregulation) to red (upregulation).

(C) (Left) Immunocytochemistry of hiPSC-NPC at D0, with the expression of nestin, vimentin, and Sox-2. Scale bars, 50 μm. (Right) Confocal imaging of neurospheroids at D30, with staining of βIII-tubulin or dendritic MAP2 and presynaptic markers of GABAergic (GAD65/67-positive) and glutamatergic (VGlut1-positive) neurons (3D-rendering insets of regions indicated by the asterisks highlight co-localization), βIII-tubulin, and glial fibrillary acidic protein (GFAP). Scale bars, 10 μm.

(D) Top ten canonical pathways identified by IPA to describe the transcriptome modulation between D0 and D30.

(E) Two-dimensional annotation enrichment analysis, correlating the pathways significantly modulated during 3D differentiation at the transcriptome and proteome level (Benjamini-Hochberg FDR < 0.05). Negative score values describe downregulation and positive scores indicate upregulation. Each dot represents a GO-Biological Process (GO-BP) term. Related GO-BP terms are presented with the same color.

(legend continued on next page)

percentage of actively proliferating cells was observed, with only 2% of cells staining positively for EdU at day 30 (Figure S1O), suggesting differentiation into post-mitotic cell populations. Cell density remained fairly constant despite the reduction in cell proliferation, further supporting the high cell viability observed along the culture time course (Figure S1M).

Transcriptomic (RNA sequencing [RNA-seq]) and proteomic (SWATH-mass spectrometry [MS]) analyses were performed in samples from four independent cultures (two from each cell line), identifying and quantifying 28,206 transcripts and 3,728 proteins. The replicates both at transcriptome and proteome levels revealed good correlation and low inter-cell line variability, as demonstrated by the Pearson correlation coefficient (PCC) higher than 0.9 (Figures S2A and S2B, respectively). For approximately 98% of the identified proteins we could also quantify the transcript abundance (Figure 1B). From these datasets, the most represented cellular compartments were cytoplasm and nucleus, which together consisted of 37.5% and 79% of the identified transcripts and proteins, respectively (Figure 1C). Approximately 15% of the identified transcripts and proteins were classified as associated with the extracellular space and plasma membrane compartments (Figure 1C).

Next, we compared the changes induced by the 3D differentiation in the transcriptome and proteome. Looking to the fold changes between day 0 and day 30, a good correlation between transcript and protein was obtained (PCC of 0.63; Figure 1D). However, when we analyzed the different time points individually, a higher PCC was obtained for day 0 (0.60) in comparison with the samples from 3D differentiation (0.46 and 0.49, respectively, for day 12 and day 30; Figure S2).

Pathway Modulation during 3D Differentiation

Hierarchical clustering of transcriptomic data revealed that the samples from early (day 12) and late (day 30) differentiation stages clustered together, indicating a higher degree of similarity in gene expression profile relative to non-differentiated cultures (day 0), which were in a more distant cluster (Figure 2A). This suggests that an intense remodeling occurs early in time defining the commitment toward the neuronal and glial lineages, as demonstrated by the upregulation of lineage-specific markers (Figure 2B). The transition from progenitors toward neuronal and astrocytic cells was also evident by immunofluorescence (Figure 2C). Most cells were positive for the NPC markers nestin, vimentin, and SOX2 at day 0, while differentiated neurospheres (day 30) were highly enriched in neuronal (βIII-tubulin-positive) and glial (GFAP-positive) lineage cells (Figure 2C). Concerning neuronal differentiation, vGlut1- and GAD65/67-positive neuronal populations were also detected at day 30, suggesting the presence of glutamatergic and GABAergic neurons, respectively (Figure 2C).

The main modulated pathways and networks between day 0 and day 30 were identified by analyzing the transcriptomic dataset. The resulting top ten canonical pathways highlight the over-representation of neuronal differentiation pathways, such as cyclic AMP (cAMP) and CREB signaling (Figure 2D). Other pathways related to neuronal morphogenesis were also among the most represented pathways, namely Ephrin and RhoGDI signaling. Genes associated with establishment of excitatory glutamatergic and inhibitory GABAergic synaptic machineries were highly enriched in the obtained datasets, consistent with the immunofluorescence observations (Figure 2C). Concerning regional identity, neurospheroids presented a mixed phenotype with expression of genes associated with development of forebrain, midbrain, and hindbrain (Figures S3A and S3B). Furthermore, correlation analysis with brain tissue data revealed a higher correlation with cortical structures, to the detriment of thalamus and cerebellum (Figure S3C). This was also in line with the upregulation of several telencephalic markers observed during neurospheroid differentiation, in which no clear trend was observed toward dorsal or ventral identity (Figures S3D and S3E).

The correlation between the transcriptome and proteome data in terms of main modulated pathways was evaluated by gene ontology (GO) enrichment analysis. Both datasets were well correlated in terms of significantly modulated biological processes (GO-BP), as shown by the two-dimensional annotation enrichment analysis (Figure 2E). The obtained data demonstrated that synaptic machinery, neural development, and cell signaling related processes were upregulated during 3D differentiation both at transcriptome and proteome level. Most downregulated pathways were associated with cellular proliferation,

(F) Proposed regulatory network responsible for the transcriptome remodeling during differentiation. Different factors were color labeled according to the fold change between D0 and D30, ranging from green (downregulation) to red (upregulation). Predicted activation *Z* score is indicated by the number bellow each of the three transcription factors (*REST*, *ASCL1*, and *TLX3*), where negative and positive values indicate repression and activation, respectively.

(G) Transcript levels of the different players represented in the regulatory network. Data are presented as mean ± SEM of the $\log_2$ of the fold change between D0 and D12 (green bars) or D0 and D30 (orange bars). Data shown in all panels represent four pooled independent biological experiments (two independent experiments of two cell lines).

See also Figures S1 and S3; Table S1.

such as cell cycle, gene expression, and primary metabolism/biosynthesis related processes, suggesting a progression in the developmental pathways toward mature post-mitotic neural cell populations. This is consistent with the EdU proliferation assay data (Figure S1O) and with the modulation of cyclin-dependent kinase (CDK) expression. *CDK1*, *CDK4*, and *CDK7*, which govern cell-cycle progression, were downregulated while *CDK5* was upregulated (Figure S1P).

The transcriptomic dataset was used to infer the main transcription factors responsible for the modulation observed during neurospheroid differentiation (Figure 2F). We found the repression of *REST* and the activation of *ASCL1* and *TLX3* to play a pivotal role in driving the transcriptional changes observed. The activity modulation of these transcription factors induced the expression of neurogenic genes, such as *ASCL1*, *NEUROG2*, and *TLX3*. Concomitantly, this orchestrated signaling network also included the repression of important cell-cycle modulators, such as *PLK1*, *BRIP1*, and *HIST1H2BJ*. Analyzing the fold changes in the expression levels of this network's players, we observed that these different molecules are regulated early (day 12) in the differentiation process, exerting its downstream effects along the culture time course (Figure 2G).

ECM and Plasma Membrane Remodeling in 3D Cultures

To address our hypothesis that the neurospheroid differentiation would induce a cell microenvironment with higher similarity to what is observed *in vivo*, we compared the proteome of neurospheroid cultures with 2D cultures after 30 days of differentiation. Principal component analysis (PCA) revealed a clear separation between the neurospheroid and 2D differentiated experimental groups; nonetheless, the 2D differentiated group was closer to neurospheroids at day 12 than at day 30 (Figure S4A). Hierarchical clustering of the significantly modulated proteins between the different experimental groups showed that all of the differentiated groups were clustering together and away from the non-differentiated day 0 (Figure S4B). However, when we filtered the proteome dataset only for proteins annotated as part of the extracellular space and plasma membrane (according to the Ingenuity Pathway Analysis [IPA] knowledge base), we observed a shift in the hierarchical clustering of the different groups: the 2D differentiated group clustered together with day 0, while the 3D differentiated groups were in a separate cluster.

A direct comparison of the total proteome of neurospheroids and 2D cultures at day 30 revealed that there were 663 and 513 proteins specifically enriched in neurospheroids or 2D, respectively (Figure 3B). This differential protein expression corresponded to a significant enrichment in GO-BP terms associated with cell signaling, synaptic machinery, and cell morphogenesis/migration in neurospheroids. On the other hand, 2D differentiation resulted in enrichment of GO-BP terms related to ECM organization/regulation, namely collagen fibril organization and collagen metabolic process (Figure 3C).

Analyzing the extracellular space and plasma membrane proteome, several functional categories were found to be significantly enriched, namely secreted proteins, ECM, cell adhesion, cell junction, cell projection, synapse, and ion transport (Figures 3D and S6A). Closer inspection of these categories showed significant differences in the ECM composition of neurospheroids and 2D differentiated cultures. Neurospheroid cultures presented low levels of collagens and high levels of the proteoglycans BCAN, VCAN, and HSPG2 and the link protein TNC (Figure 3E). LAMA4, the only laminin subunit found to be enriched in neurospheroids, has been predicted to play a relevant role during neural development (Chen et al., 2015). 2D cultures presented a collagen-rich ECM, with the upregulation of different subunits of collagen types I, V, VI, and XII, collagen-interacting proteins (SPARC and CRTAP), and ANXA2, which can mediate collagen secretion (Dassah et al., 2014). Integrin receptors responsible for binding basement membrane ECM components, such as ITGA6, ITGB1, and ITGAV, were also enriched in 2D.

Analyzing the profile of differentially expressed cell adhesion molecules, we observed that most of the proteins enriched in neurospheroids are key players in neural development and morphogenesis. These include several neural cell adhesion molecules (CAMs), known to mediate axon guidance/outgrowth by modulating neuron-ECM interaction and attraction/repulsion properties (PCDH1, NEO1, EPHB1, NRXN2, ADGRG1, CDH13, NRCAM, LSAMP, NCAM1, NFASC, NEGR1, CNTN1, NECTIN1, and CTNNA2) (Figure 3E). Structural synaptic machinery proteins were significantly enriched in neurospheroids, including NECTIN1, NRXN2, NLGN2, SHANK2, HOMER1, GPHN, and CADM1–CADM4. Moreover, proteins related with synaptic vesicle trafficking and neurotransmitter release were also found in higher abundance in neurospheroids, including SYN1, VAMP2, SNAP25, STXBP5, LIN7A, SYNGR1, SYNGR3, CADPS, and AMPH. Similar observations were made for proteins involved in ion transport, as the expression of several Na^+/K^+-ATPase subunits (ATP1A1, ATP1A3, ATP1B1, ATP1B3, ATP2B2, and ATP2B4) are essential in maintaining the resting potential at the expense of large ATP amounts. Among these different subunits, ATP1B3 was the only one that was present in similar abundance levels between day 0 and day 30 in neurospheroids, which is in line with previous observations in primary murine NPC *in vitro* neuronal differentiation (Frese et al., 2017).

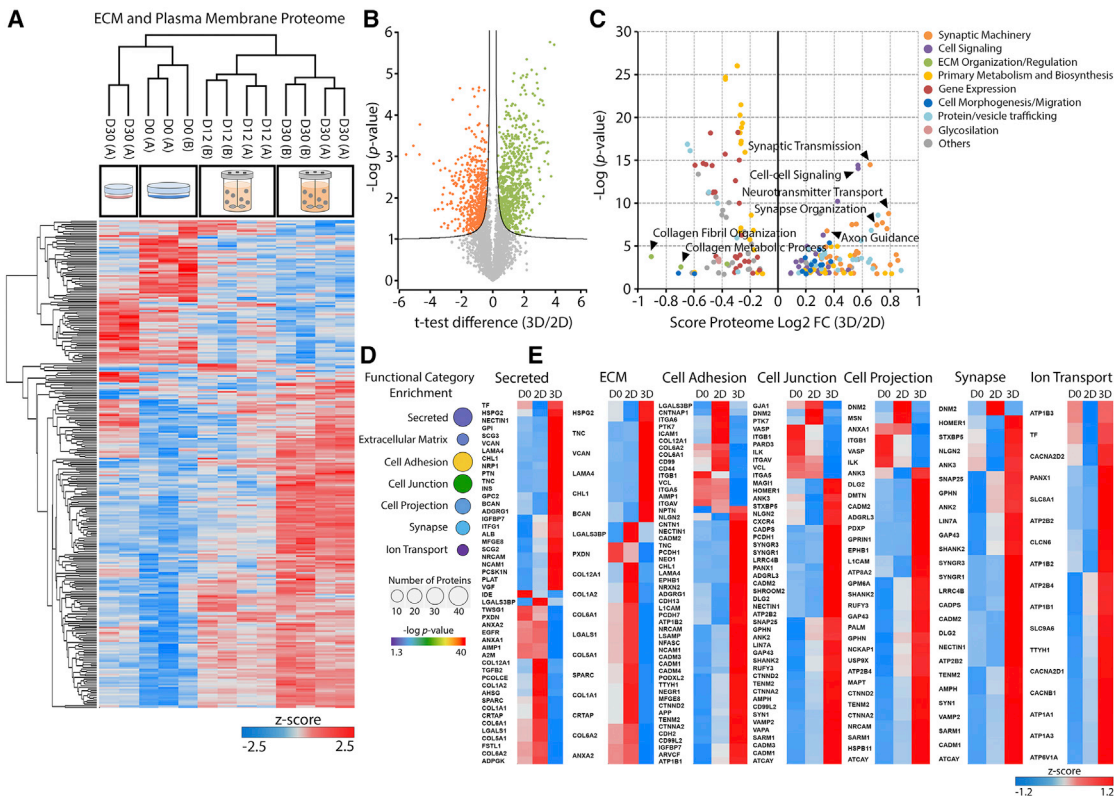

Figure 3. Extracellular Space and Plasma Membrane Proteome Remodeling during hiPSC-NPC 3D Differentiation

(A) Heatmap of proteins significantly modulated at the extracellular or plasma membrane level, during 3D and 2D differentiation (total of 294 proteins). Hierarchical clustering performed for the biological replicates of each time point and cell line (in columns) and for proteins (in rows). Significantly modulated proteins identified by multi-sample ANOVA test with a permutation-based FDR cutoff of 0.05 applied on the logarithmized intensities. *Z* score values were color coded from blue (downregulation) to red (upregulation).

(B) Volcano plot of proteins identified after 2D or 3D differentiation of hiPSC-NPCs. Significantly enriched proteins after 2D (orange) or 3D (green) differentiation are color labeled. Significantly modulated proteins identified by permutation-based FDR t test applied on the logarithmized intensities, with a threshold value of 0.05 and S0 of 0.1.

(C) GO-BP terms significantly over-represented (Benjamini-Hochberg FDR < 0.02) in 2D (negative score) or 3D (positive score) differentiated cells. The y axis presents the corresponding p values (in negative log scale). Related GO-BP terms are presented with the same color, where some specific terms are highlighted by arrowheads.

(D) Selected functional categories significantly over-represented during 3D differentiation (Benjamini-Hochberg FDR < 0.05) for proteins annotated as extracellular space or plasma membrane components. p values and number of proteins are graphically represented by different colors and sphere sizes, respectively.

(E) Heatmaps of protein abundance profile at day 0 (D0), 2D at day 30, and 3D at day 30 of selected categories. *Z* score values were color coded from blue (downregulation) to red (upregulation). Data shown in all panels represent four (two independent experiments of two cell lines) or two pooled independent biological experiments, for neurospheroids or 2D cultures, respectively.

See also Figure S4 and Table S2.

The majority of the observations on proteomics data were further supported by the transcriptomic analysis, whereby similar trends in fold changes of neurospheroids between day 0 and day 30 were observed at transcript level for most of the differentially expressed proteins (Figure S4D). Moreover, we further confirmed the accumulation of TNC and the CNS-specific proteoglycans, BCAN and NCAN, in neurospheroids by immunostaining and wisteria floribunda agglutinin labeling (Figures S4E and S4F). NCAN, although not quantified in our proteomic dataset, was found to be significantly upregulated at transcript level.

Impact of Culture System on Neuronal Differentiation

To further validate our findings, we compared our datasets with publicly available data obtained from neural differentiation of human stem cells in different culture systems. The dataset from Srikanth et al. (2015) allowed a

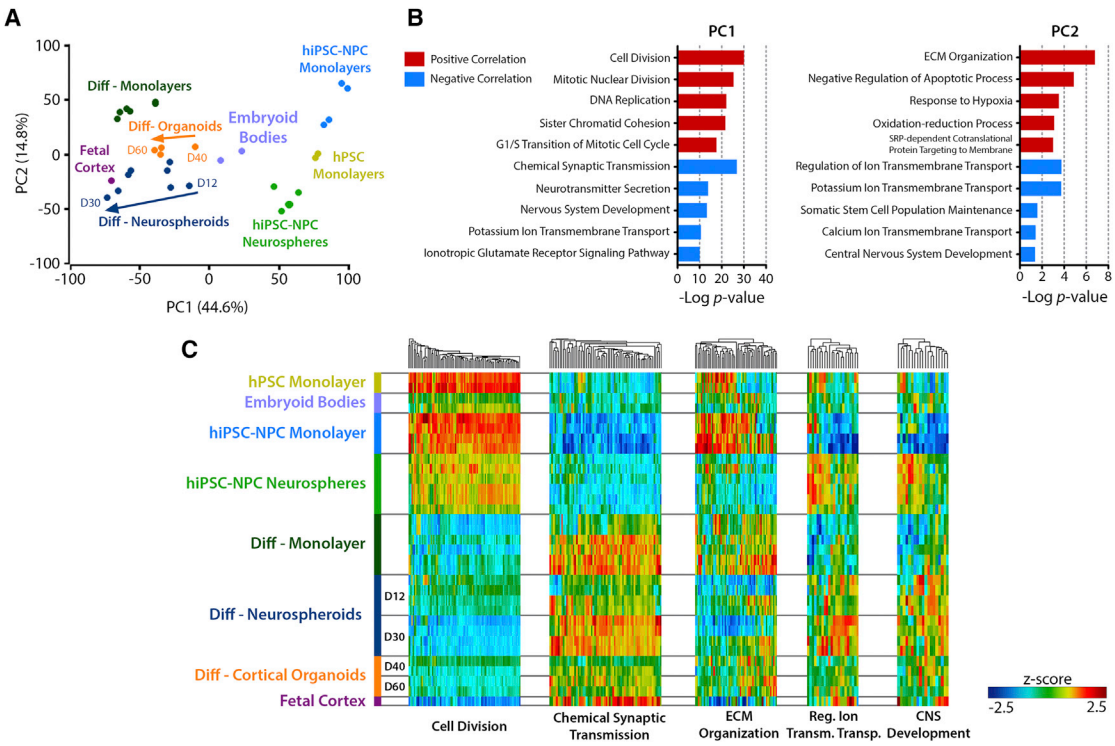

Figure 4. Transcriptomic Remodeling during Neural Differentiation in Different 2D and 3D Culture Systems

(A) Principal component analysis of different *in vitro* culture systems.

(B) Main GO-BP terms significantly over-represented in genes with top 1,000 positive (red) or negative (blue) loadings for principal component 1 (PC1) or PC2. The y axis corresponds to the negative $\log_{10}$ of the p values (FDR corrected).

(C) Heatmap of the genes included in the GO-BP terms of cell division (87 genes), chemical synaptic transmission (68 genes), ECM organization (59 genes), regulation of ion transmembrane transport (22 genes), and CNS development (19 genes). Hierarchical clustering was performed for different genes (columns). Rows represent the different samples. *Z* score values were color coded from blue (down-regulation) to red (upregulation).

See also Table S3.

comparison with hiPSC-NPC cultured as proliferative neurospheres and their neural differentiation as 2D monolayers. For comparison with human pluripotent stem cell (hPSC) cultures expanded in 2D cultures, embryoid bodies, Matrigel-embedded cortical organoids, and fetal cortex (male, 19 weeks gestation), we used the dataset from Luo et al. (2016). All samples were normalized and compared through PCA, where most of the variance could be explained by PC1 (44.6%) and PC2 (14.8%) (Figure 4A). PC1 revealed a clear separation between the undifferentiated stem cell samples (hPSCs and hiPSC-NPCs) and the differentiated samples. Among the differentiated samples, neurospheroids from day 30 were the samples with a profile closest to that of the fetal cortex.

Next, we analyzed the genes associated with the top PCA loadings contributing to PC1 and PC2 scores (Figure 4B). PC1 positive scores were mostly correlated with the high expression levels of cell-cycle progression genes in proliferating hPSCs and hiPSC-NPCs (Figures 4B and 4C). However, hiPSC-NPCs cultured as proliferative neurospheres present a lower activation of these genes, which is in line with many other cell types that have lower proliferation rates when cultured in 3D systems (Edmondson et al., 2014). All differentiated samples demonstrated a repression of these cell-cycle-associated genes, whereby the fetal cortex presented the lowest expression levels followed by neurospheroids at day 30. PC1 negative scores were highly correlated with nervous system development and synaptic maturation/function. Analyzing the cluster of genes associated with chemical synaptic transmission, we observed that these were highly upregulated in neurospheroids at day 30 and in differentiated monolayers, while displaying lower levels in the cortical organoid samples. Furthermore, these results on chemical synaptic transmission related genes are also supported by the correlation of PC2 negative scores with genes related to regulation of ion transmembrane transport, comprising several potassium and calcium

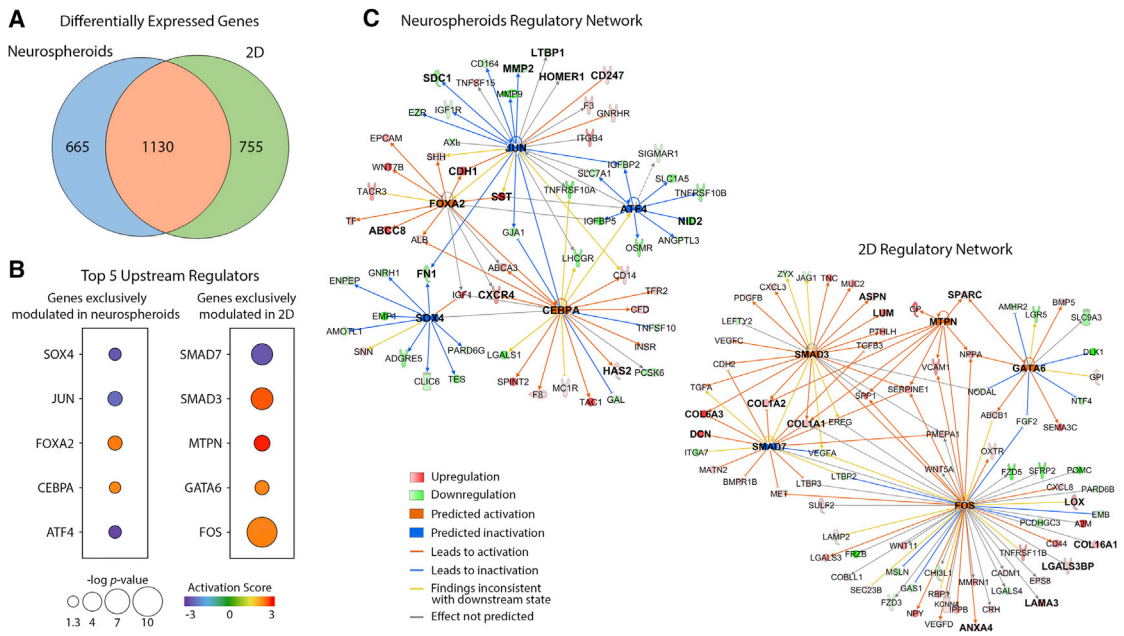

Figure 5. Upstream Regulator Analysis of Neurospheroids and 2D Differentiation

(A) Venn diagram of differentially expressed genes associated with extracellular space and plasma membrane in neurospheroids and 2D differentiation (Srikanth et al., 2015).

(B) Top five upstream regulators predicted in IPA to be responsible for the differential gene expression of exclusively modulated genes (extracellular space and plasma membrane genes only) in 3D (665 genes) and 2D (755 genes). The activation scores and p values are graphically represented by different colors and sphere sizes, respectively.

(C) Regulatory networks derived for 3D and 2D data based on IPA predictions for the top five upstream regulators.

See also Figure S5.

voltage-gated channels critical for synaptic function. These genes were also more enriched in neurospheroids, as compared with monolayers or cortical organoids (Figure 4C). PC2 positive scores were found to be mostly correlated with ECM organization processes, which include several genes encoding for basement membrane components (collagens and laminins) and CAMs (integrins). This gene cluster was more enriched in monolayer cultures of hNPCs and 2D differentiated cells, presenting very low expression levels in fetal cortex. 3D cultures presented an intermediate expression profile for this cluster, still with neurospheroids presenting lower expression of collagen- and laminin-related genes relative to cortical organoids. The CNS development cluster identified in PC2 negative correlation includes some of the main structural neural ECM components, such as the proteoglycans aggrecan, brevican, and neurocan, which were found to have higher expression levels in 3D differentiated cultures (neurospheroids and organoids), relative to differentiation in monolayer (Figure 4C). The CNS-specific hyaluronan binding link proteins *HAPLN2* and *HAPLN4* were expressed at higher levels on neurospheroids relative to cortical organoids.

To compare and highlight the differences between the expression profiles of genes encoding for extracellular space and plasma membrane proteins in neurospheroids and 2D differentiated samples, we used IPA to predict the most relevant upstream regulators in each dataset. Of the top five transcription factors identified for the neurospheroids dataset, three presented similar activation scores to the 2D dataset (*TLX3*, *REST*, and *ASCL1*), while two were only predicted to be activated on neurospheroids (*PTF1A* and *MITF*) (Figure S5).

Among the differentially expressed genes associated with extracellular space and plasma membrane in 3D and 2D, 1,130 genes were modulated in both datasets while 665 and 755 genes were exclusively modulated on neurospheroids and 2D differentiation, respectively (Figure 5A). We focused on these two lists of exclusively modulated genes to address in more detail the differences between 3D and 2D differentiation, by identifying the most significant upstream regulators (Figures 5B and 5C). The top five identified regulators in neurospheroids play a relevant role in modulating the expression of ECM genes. *CEBPA*, which was predicted to be activated, is known to drive the expression of *HAS2* in neuronal cells, in agreement with the

upregulation observed for this gene in neurospheroids. Conversely, downregulation of fibronectin 1 encoding gene (*FN1*) was predicted to be mediated by the inactivation of *JUN* and *SOX4*. *JUN* was also predicted to be involved in the downregulation of other ECM modulators, namely *LTBP1*, *MMP2*, and *SDC1*. Moreover, *FOXA2* and *JUN* were involved in the upregulation of genes associated with synaptic machinery and dendritic spine morphogenesis, such as *ABCC8*, *CDH1*, *SST*, *HOMER1*, and *CD247*. *CEBPA* and *FOXA2* were also predicted to activate the expression of the neuronal migration regulator *CXCR4*.

The regulatory network derived for the 2D cultures revealed that four out of the top five transcription regulators had a relevant role on the upregulation of laminin- and collagen-encoding genes (*LAMA3*, *COL1A1*, *COL1A2*, *COL6A3*, and *COL16A1*), namely the predicted activation of *SMAD3*, *FOS*, and *MTPN* and inactivation of *SMAD7*. The upregulation of *ANXA4*, *LGALS3BP*, predicted to be under the control of *FOS*, was also in agreement with our proteomics data for 2D differentiation described above.

DISCUSSION

Neural microenvironment homeostasis plays an essential role in the maintenance of normal cellular function in CNS. Here, we addressed the cellular and extracellular remodeling occurring *in vitro* during 3D differentiation of hiPSC-NPCs, in a system devoid of exogenous ECM addition (e.g., Matrigel): neurospheroids differentiated in perfusion stirred-tank bioreactors. Changes in the expression patterns were analyzed via a two-level integrative approach, generating a large-scale quantitative transcriptome and proteome dataset. Such approaches can, for instance, highlight the contribution of non-genetic regulation mechanisms (Low et al., 2013; Sacco et al., 2016). Post-transcriptional regulation plays a critical role during neural development, namely in neuronal morphogenesis and connectivity (DeBoer et al., 2013; Frese et al., 2017). Our datasets reflect the relevance of post-transcriptional control mechanisms during neural differentiation compared with the neural progenitor cell state, with lower correlation coefficients being observed between mRNA and protein levels once neurospheroid differentiation started.

A global overview of the transcriptional changes occurring during neurospheroid differentiation revealed that these were mostly related to the modulation of cAMP, RhoGDI, and Ephrin signaling pathways. These pathways are well-known for their role during neurogenesis, regulating neuronal morphogenesis, survival, and migration (Hall and Lalli, 2010; Klein, 2004; Lonze and Ginty, 2002). The main transcriptional regulation predicted to be driving these modulations was the repression of REST, which is consistent with its function as a negative neurogenesis regulator (Palm et al., 1998). The observed upregulation of *SRRM4* was identified as one possible contributor to *REST* repression, by promoting the expression of a less active truncated *REST* isoform via alternative splicing (Raj et al., 2011). The decreased *REST* repressive activity results in increased expression of *ASCL1*, *NEUROG2*, and *TLX3*, which are essential players in the development and specification of neuronal lineages (Borromeo et al., 2014; Casarosa et al., 1999; Parras et al., 2002). These transcriptional changes were followed by a gradual arrestment of the cell cycle, suggesting a progression toward mature post-mitotic neural cell populations. The neuronal cell-cycle suppressor *CDK5* and its activator *CDK5R1*, which are typically expressed in post-mitotic neurons (Frese et al., 2017; Zhang and Herrup, 2011), were found to be upregulated during neurospheroid differentiation. Correlation with human brain tissue data revealed that the generated neurospheroids displayed higher similarity with cortical structure expression, despite the expression of fore-, mid-, and hindbrain developmental genes. To further elucidate the impact of regional identity on the expression patterns of ECM-associated genes, we adapted region-directed differentiation protocols (Ashton et al., 2015; Niclis et al., 2017; Yuan et al., 2016) for neurospheroid differentiation.

Our data show that neurospheroid differentiation induces a significant modulation of ECM components and CAMs, diverging greatly from the profile resulting from 2D differentiated cultures. Here, a distinct feature between both differentiation processes was the enrichment in neurospheroids of several PNN components, including proteoglycans (BCAN and VCAN), and link protein TNC, as well as increased gene expression of *TNR* and hyaluronan synthesis/binding proteins (*HAS2*, *HAPLN2*, and *HAPLN4*) (Yamaguchi, 2000). In addition to structural ECM components, the expression profile of cell surface proteins also diverged considerably between neurospheroids and monolayers. NRCAM, NFASC, L1CAM, and CHL1, key modulators of axon guidance (Maness and Schachner, 2007; Sakurai, 2012), were enriched in neurospheroids relative to 2D cultures. Several synaptic machinery proteins were also significantly enriched in neurospheroids, such as CAMs, which have been described as essential for synapse morphogenesis and organization. These include NCAM1, whose role in both early synaptogenesis and subsequent synaptic maturation is well documented; the presynaptic proteins NECTIN1 and NRXN2; the post-synaptic proteins NLGN2, SHANK2, HOMER1, and GPHN; and the four trans-synaptic CADM proteins CADM1, CADM2, CADM3, and CADM4 (Dityatev, 2004; Fogel et al., 2007; Togashi et al., 2009).

In contrast, 2D differentiation resulted in a collagen-rich ECM, which may result from signaling cues provided by the laminin-coated surfaces and by different stiffness,

mechanical properties, or cell-cell interactions (e.g., neuron-astrocyte), relative to 3D cultures. This collagen-enriched profile suggests that 2D cultures offer a more distant representation of the healthy neural tissue microenvironment as compared with the profile obtained in the neurospheroids. Collagen deposition in neural tissue is often associated with pathological alterations, promoted for instance by gangliomas that induce the expression of many collagen-interacting proteins that were enriched in the 2D differentiated cultures (e.g., PXDN, LGAL1, LGALS3BP, A2M, ANXA4, and ITGA5) (Autelitano et al., 2014; Liu et al., 2010; Le Mercier et al., 2010).

To minimize any possible bias in the analysis and to increase the significance of our findings, we further compared our datasets with publicly available data derived from different protocols for 3D and 2D neural differentiation and fetal cortex tissue. The current limitations on standardized methods for proteome quantification and data availability hampered comparison studies at protein level between different *in vitro* protocols and/or tissue samples but allowed comparisons at transcriptome levels. This comparative analysis further supported our previous observations on the microenvironment differences between 3D and 2D systems. ECM organization-related genes were among the most significant genes contributing to the separation of 2D and 3D biological samples in the PCA. Similarly to what we observed for neurospheroids, cortical organoids and fetal cortex displayed lower expression levels of collagen- and laminin-related genes and increased the expression of neural proteoglycan-encoding genes, relative to 2D cultures. Between the two 3D systems, neurospheroids presented increased expression of genes related to synaptic machinery and ion channels. The higher intra- and inter-spheroid homogeneity (Simão et al., 2015) compared with cortical organoids (Lancaster and Knoblich, 2014; Lancaster et al., 2013) can contribute to these differences.

As in the neurospheroid differentiation process, *REST* repression together with *TLX3* and *ASCL1* activation were among the most relevant transcriptional regulators predicted to be driving the neural differentiation in 2D cultures. Still, the analysis of upstream regulators modulating the expression of ECM and plasma membrane related genes in neurospheroids and 2D cultures revealed clear differences between both systems. In the neurospheroids *JUN* and *ATF4* were predicted to be repressed, inducing the downregulation of molecules such as *LTBP1*, *MMP2*, *SDC1*, and *NID2* that regulate collagen biosynthesis, processing, and binding (Hori et al., 1998; Ishikawa and Kramer, 2010; Kohfeldt et al., 1998; Visse, 2003). The activation of *CEBPA* and *FOXA2* regulated the upregulation of several synaptic proteins and the chemokine receptor *CXCR4*, key player during neuronal differentiation and migration (Pitcher et al., 2010). For 2D differentiation, all the identified transcription factors are involved in modulating the expression of collagens and collagen processing/organization proteins, including *LUM*, *ASPN*, *LOX*, *SPARC*, and *DCN* (Chakravarti et al., 1998; Lau et al., 2006; Nakajima et al., 2007).

Human 3D *in vitro* models, such as the neurospheroids described herein and cortical organoids, can be valuable tools to enable better understanding of the dynamics of ECM and soluble factor secretion/degradation. The two 3D culture methods present specific advantages and drawbacks, making them more suited for different applications. As demonstrated by several authors, cortical organoids, employing the methodology first published by Lancaster et al. (2013), are well suited to address questions regarding the human neurodevelopmental process (Akkerman and Defize, 2017). However, these structures typically present high batch-to-batch variability, rendering it less adequate for drug or toxicological screening. Neurospheroids present a simpler structure and are devoid of exogenous ECM addition. Thus, the increased homogeneity between individual structures and different batches makes it a more suitable system for preclinical applications and with potential to address disease-associated modulation of neuron-ECM interactions. Large-scale quantitative approaches, such as the one presented in this work, can be applied to address the link between changes in neural microenvironment and neurological disorders. The amount of evidence suggesting this link is increasing, including for instance the ECM remodeling following brain injury induced by reactive astrocytes (e.g., traumatic brain injury, stroke) (Kim et al., 2016; Zamanian et al., 2012).

Overall, we have demonstrated that the 3D differentiation of hNPCs as neurospheroids induces the expression of important cellular and extracellular proteins typically observed in the neural tissue. By combining a comprehensive transcriptomic and proteomic characterization, we demonstrate that neurospheroid cultures can better mimic the protein composition of the neural microenvironment as compared with the traditional monolayer-based cell models. The extension of this culture system to other cell sources (e.g., patient-derived iPSCs) and/or chemical and physical insults is therefore likely to contribute to a more accurate assessment of the role and link between ECM changes and neurological disorders.

EXPERIMENTAL PROCEDURES

Generation of Neural Progenitors from Human Induced Pluripotent Stem Cells and Differentiation

Human iPSCs (Royan iPSC clone 1 [R1-hiPSC1] and clone 4 [R1-hiPSC4], also known as RIi001-A and RIi007-A, respectively) were derived from dermal fibroblasts as described previously (Totonchi et al., 2010). Neural progenitor cells generation, differentiation,

and immunostaining were performed as described in Supplemental Experimental Procedures.

Quantitative Transcriptomics and Proteomics

All samples were processed for RNA-seq and SWATH-MS as described in Supplemental Experimental Procedures. Computational and statistical analysis of the datasets was performed using Perseus software environment (Tyanova et al., 2016), DAVID 6.8 (Huang et al., 2009), and IPA, as described in Supplemental Experimental Procedures.

ACCESSION NUMBERS

Data have been deposited at the Gene Expression Omnibus (https://www.ncbi.nlm.nih.gov/geo) and Proteome Xchange Consortium via PRIDE (Vizcaíno et al., 2016). GEO: GSE102139 (RNA-seq); Proteome Xchange: PXD007130 (SWATH-MS).

SUPPLEMENTAL INFORMATION

Supplemental Information includes Supplemental Experimental Procedures, five figures, and three tables and can be found with this article online at https://doi.org/10.1016/j.stemcr.2018.06.020.

AUTHOR CONTRIBUTIONS

Conceptualization, D.S. and C.B.; Methodology, D.S., P.G.-A., N.R., and C.B.; Formal Analysis, D.S., P.G.-A., and N.R.; Investigation, D.S., M.M.S., A.P.T., and F.A.; Writing – Original Draft, D.S. and C.B.; Writing – Review & Editing, D.S., P.G.-A, N.R., and C.B.; Visualization, D.S.; Resources, M.F.Q.S., N.Z.M., T.S., N.R., P.G.-A., and P.M.A.; Funding Acquisition, N.R., P.M.A., and C.B.; Supervision, P.M.A. and C.B.

ACKNOWLEDGMENTS

iNOVA4Health – UID/Multi/04462/2013, a program financially supported by Fundação para a Ciência e Tecnologia/Ministério da Educação e Ciência, through national funds and co-funded by FEDER under the PT2020 Partnership Agreement, is acknowledged. PD/BD/52473/2014, PD/BD/52481/2014, and PD/BD/128371/2017 PhD fellowships funded by FCT, Portugal. N.R. is supported by the European Research Council Starting Grant 337327. T.S. is supported by a grant provided by the Deutsche Forschungsgemeinschaft (DFG) (grant number SA 1382/7-1). The authors gratefully thank João Clemente for support on the bioreactor operation and Dr. Inês Isidro for fruitful discussions on data analysis. MS data were obtained by UniMS – Mass Spectrometry Unit, ITQB/iBET, Oeiras, Portugal.

Received: November 8, 2017
Revised: June 25, 2018
Accepted: June 27, 2018
Published: July 26, 2018

REFERENCES

Akkerman, N., and Defize, L.H.K. (2017). Dawn of the organoid era: 3D tissue and organ cultures revolutionize the study of development, disease, and regeneration. BioEssays *39*. https://doi.org/10.1002/bies.201600244.

Ashton, R., Lippmann, E., Estevez-Silva, M., and Ashton, R. (2015). Chemically defined differentiation of human pluripotent stem cells to hindbrain and spinal cord neural stem cells with defined regional identities. Protocol Exch. https://doi.org/10.1038/protex.2015.076.

Autelitano, F., Loyaux, D., Roudières, S., Déon, C., Guette, F., Fabre, P., Ping, Q., Wang, S., Auvergne, R., Badarinarayana, V., et al. (2014). Identification of novel tumor-associated cell surface sialoglycoproteins in human glioblastoma tumors using quantitative proteomics. PLoS One *9*, e110316.

Bandtlow, C.E., and Zimmermann, D.R. (2000). Proteoglycans in the developing brain: new conceptual insights for old proteins. Physiol. Rev. *80*, 1267–1290.

Bikbaev, A., Frischknecht, R., and Heine, M. (2015). Brain extracellular matrix retains connectivity in neuronal networks. Sci. Rep. *5*, 14527.

Borromeo, M.D., Meredith, D.M., Castro, D.S., Chang, J.C., Tung, K.-C., Guillemot, F., and Johnson, J.E. (2014). A transcription factor network specifying inhibitory versus excitatory neurons in the dorsal spinal cord. Development *2812*, 2803–2812.

Casarosa, S., Fode, C., and Guillemot, F. (1999). Mash1 regulates neurogenesis in the ventral telencephalon. Development *126*, 525–534.

Chakravarti, S., Magnuson, T., Lass, J.H., Jepsen, K.J., LaMantia, C., and Carroll, H. (1998). Lumican regulates collagen fibril assembly: Skin fragility and corneal opacity in the absence of lumican. J. Cell Biol. *141*, 1277–1286.

Chen, L., Chu, C., Kong, X., Huang, T., and Cai, Y.D. (2015). Discovery of new candidate genes related to brain development using protein interaction information. PLoS One *10*, 1–11.

Dassah, M., Almeida, D., Hahn, R., Bonaldo, P., Worgall, S., and Hajjar, K.A. (2014). Annexin A2 mediates secretion of collagen VI, pulmonary elasticity and apoptosis of bronchial epithelial cells. J. Cell Sci. *127*, 828–844.

DeBoer, E.M., Kraushar, M.L., Hart, R.P., and Rasin, M.R. (2013). Post-transcriptional regulatory elements and spatiotemporal specification of neocortical stem cells and projection neurons. Neuroscience *248*, 499–528.

Dityatev, A. (2004). Polysialylated neural cell adhesion molecule promotes remodeling and formation of hippocampal synapses. J. Neurosci. *24*, 9372–9382.

Edmondson, R., Broglie, J.J., Adcock, A.F., and Yang, L. (2014). Three-dimensional cell culture systems and their applications in drug discovery and cell-based biosensors. Assay Drug Dev. Technol. *12*, 207–218.

Fogel, A.I., Akins, M.R., Krupp, A.J., Stagi, M., Stein, V., and Biederer, T. (2007). SynCAMs organize synapses through heterophilic adhesion. J. Neurosci. *27*, 12516–12530.

Frese, C.K., Mikhaylova, M., Stucchi, R., Gautier, V., Liu, Q., Mohammed, S., Heck, A.J.R., Altelaar, A.F.M., and Hoogenraad, C.C. (2017). Quantitative map of proteome dynamics during neuronal differentiation. Cell Rep. *18*, 1527–1542.

Hall, A., and Lalli, G. (2010). Rho and Ras GTPases in axon growth, guidance, and branching. Cold Spring Harb. Perspect. Biol. *2*, 1–18.

Hori, Y., Katoh, T., Hirakata, M., Kaname, S., Fukagawa, M., Okuda, T., Ohashi, H., Fujita, T., Miyazono, K., and Kurokawa, K. (1998). Anti-latent TGF-β binding protein-1 antibody or synthetic oligopeptides inhibit extracellular matrix expression induced by stretch in cultured rat mesangial cells. Kidney Int. *53*, 1616–1625.

Howell, M.D., and Gottschall, P.E. (2012). Lectican proteoglycans, their cleaving metalloproteinases, and plasticity in the central nervous system extracellular microenvironment. Neuroscience *217*, 6–18.

Huang, D.W., Lempicki, R.A., and Sherman, B.T. (2009). Systematic and integrative analysis of large gene lists using DAVID bioinformatics resources. Nat. Protoc. *4*, 44–57.

Humpel, C. (2015). Organotypic brain slice cultures: a review. Neuroscience *305*, 86–98.

Ishikawa, T., and Kramer, R.H. (2010). Sdc1 negatively modulates carcinoma cell motility and invasion. Exp. Cell Res. *316*, 951–965.

Kim, S.Y., Porter, B.E., Friedman, A., and Kaufer, D. (2016). A potential role for glia-derived extracellular matrix remodeling in postinjury epilepsy. J. Neurosci. Res. *94*, 794–803.

Klein, R. (2004). Eph/ephrin signaling in morphogenesis, neural development and plasticity. Curr. Opin. Cell Biol. *16*, 580–589.

Kohfeldt, E., Sasaki, T., Göhring, W., and Timpl, R. (1998). Nidogen-2: a new basement membrane protein with diverse binding properties. J. Mol. Biol. *282*, 99–109.

Lancaster, M.A., and Knoblich, J.A. (2014). Generation of cerebral organoids from human pluripotent stem cells. Nat. Protoc. *9*, 2329–2340.

Lancaster, M.A., Renner, M., Martin, C.A., Wenzel, D., Bicknell, L.S., Hurles, M.E., Homfray, T., Penninger, J.M., Jackson, A.P., and Knoblich, J.A. (2013). Cerebral organoids model human brain development and microcephaly. Nature *501*, 373–379.

Lau, Y.K.I., Gobin, A.M., and West, J.L. (2006). Overexpression of lysyl oxidase to increase matrix crosslinking and improve tissue strength in dermal wound healing. Ann. Biomed. Eng. *34*, 1239–1246.

Liu, Y., Carson-Walter, E.B., Cooper, A., Winans, B.N., Johnson, M.D., and Walter, K.A. (2010). Vascular gene expression patterns are conserved in primary and metastatic brain tumors. J. Neurooncol. *99*, 13–24.

Lonze, B.E., and Ginty, D.D. (2002). Function and regulation of CREB family transcription factors in the nervous system. Neuron *35*, 605–623.

Low, T.Y., vanHeesch, S., vandenToorn, H., Giansanti, P., Cristobal, A., Toonen, P., Schafer, S., Hübner, N., vanBreukelen, B., Mohammed, S., et al. (2013). Quantitative and qualitative proteome characteristics extracted from in-depth integrated genomics and proteomics analysis. Cell Rep. *5*, 1469–1478.

Luo, C., Lancaster, M.A., Castanon, R., Nery, J.R., Knoblich, J.A., and Ecker, J.R. (2016). Cerebral organoids recapitulate epigenomic signatures of the human fetal brain. Cell Rep. *17*, 3369–3384.

Maness, P.F., and Schachner, M. (2007). Neural recognition molecules of the immunoglobulin superfamily: signaling transducers of axon guidance and neuronal migration. Nat. Neurosci. *10*, 19–26.

Le Mercier, M., Fortin, S., Mathieu, V., Kiss, R., and Lefranc, F. (2010). Galectins and gliomas. Brain Pathol. *20*, 17–27.

Nakajima, M., Kizawa, H., Saitoh, M., Kou, I., Miyazono, K., and Ikegawa, S. (2007). Mechanisms for asporin function and regulation in articular cartilage. J. Biol. Chem. *282*, 32185–32192.

Niclis, J.C., Gantner, C.W., Alsanie, W.F., McDougall, S.J., Bye, C.R., Elefanty, A.G., Stanley, E.G., Haynes, J.M., Pouton, C.W., Thompson, L.H., et al. (2017). Efficiently specified ventral midbrain dopamine neurons from human pluripotent stem cells under xeno-free conditions restore motor deficits in parkinsonian rodents. Stem Cells Transl. Med. *6*, 937–948.

Palm, K., Belluardo, N., Metsis, M., and Timmusk, T. (1998). Neuronal expression of zinc finger transcription factor REST/NRSF/XBR gene. J. Neurosci. *18*, 1280–1296.

Parras, C.M., Schuurmans, C., Scardigli, R., Kim, J., Anderson, D.J., and Guillemot, F. (2002). Divergent functions of the proneural genes Mash1 and Ngn2 in the specification of neuronal subtype identity. Genes Dev. *16*, 324–338.

Pitcher, J., Shimizu, S., Burbassi, S., and Meucci, O. (2010). Disruption of neuronal CXCR4 function by opioids: preliminary evidence of ferritin heavy chain as a potential etiological agent in neuroAIDS. J. Neuroimmunol. *224*, 66–71.

Raj, B., O'Hanlon, D., Vessey, J.P., Pan, Q., Ray, D., Buckley, N.J., Miller, F.D., and Blencowe, B.J. (2011). Cross-regulation between an alternative splicing activator and a transcription repressor controls neurogenesis. Mol. Cell *43*, 843–850.

Rutka, J.T., Apodaca, G., Stern, R., and Rosenblum, M. (1988). The extracellular matrix of the central and peripheral nervous systems: structure and function. J. Neurosurg. *69*, 155–170.

Sacco, F., Silvestri, A., Posca, D., Pirrò, S., Gherardini, P.F., Castagnoli, L., Mann, M., and Cesareni, G. (2016). Deep proteomics of breast cancer cells reveals that metformin rewires signaling networks away from a pro-growth state. Cell Syst. *2*, 159–171.

Sakurai, T. (2012). The role of NrCAM in neural development and disorders-Beyond a simple glue in the brain. Mol. Cell. Neurosci. *49*, 351–363.

Simão, D., Pinto, C., Piersanti, S., Weston, A., Peddie, C.J., Bastos, A.E.P.P., Licursi, V., Schwarz, S.C., Collinson, L.M., Salinas, S., et al. (2015). Modeling human neural functionality in vitro: three-dimensional culture for dopaminergic differentiation. Tissue Eng. Part A. *21*, 654–668.

Simão, D., Terrasso, A.P., Teixeira, A.P., Brito, C., Sonnewald, U., and Alves, P.M. (2016a). Functional metabolic interactions of human neuron-astrocyte 3D in vitro networks. Sci. Rep. *6*, 33285.

Simão, D., Arez, F., Terasso, A.P., Pinto, C., Sousa, M.F.Q., Brito, C., and Alves, P.M. (2016b). Perfusion stirred-tank bioreactors for 3D differentiation of human neural stem cells. In Bioreactors in Stem Cell Biology, K. Turksen, ed. (Springer), pp. 129–142.

Snow, A.D., Sekiguchi, R.T., Nochlin, D., Kalaria, R.N., and Kimata, K. (1994). Heparan sulfate proteoglycan in diffuse plaques of hippocampus but not of cerebellum in Alzheimer's disease brain. Am. J. Pathol. *144*, 337–347.

Soleman, S., Filippov, M.A., Dityatev, A., and Fawcett, J.W. (2013). Targeting the neural extracellular matrix in neurological disorders. Neuroscience *253*, 194–213.

Srikanth, P., Han, K., Dana, G., Kosik, K.S., Dennis, J., Youngpearse, T.L., Srikanth, P., Han, K., Callahan, D.G., Makovkina, E., et al. (2015). Genomic DISC1 disruption in hiPSCs alters Wnt signaling and neural cell fate article genomic DISC1 disruption in hiPSCs alters Wnt signaling and neural cell fate. Cell Rep. *12*, 1414–1429.

Togashi, H., Sakisaka, T., and Takai, Y. (2009). Cell adhesion molecules in the central nervous system. Cell Adh. Migr. *3*, 29–35.

Totonchi, M., Taei, A., Seifinejad, A., Tabebordbar, M., Rassouli, H., Farrokhi, A., Gourabi, H., Aghdami, N., Hosseini-Salekdeh, G., and Baharvand, H. (2010). Feeder- and serum-free establishment and expansion of human induced pluripotent stem cells. Int. J. Dev. Biol. *54*, 877–886.

Tyanova, S., Temu, T., Sinitcyn, P., Carlson, A., Hein, M.Y., Geiger, T., Mann, M., and Cox, J. (2016). The Perseus computational platform for comprehensive analysis of (prote)omics data. Nat. Methods *13*, 731–740.

Visse, R. (2003). Matrix metalloproteinases and tissue inhibitors of metalloproteinases: structure, function, and biochemistry. Circ. Res. *92*, 827–839.

Vizcaíno, J.A., Csordas, A., Del-Toro, N., Dianes, J.A., Griss, J., Lavidas, I., Mayer, G., Perez-Riverol, Y., Reisinger, F., Ternent, T., et al. (2016). 2016 update of the PRIDE database and its related tools. Nucleic Acids Res. *44*, D447–D456.

Wang, D., and Fawcett, J. (2012). The perineuronal net and the control of CNS plasticity. Cell Tissue Res. *349*, 147–160.

Yamaguchi, Y. (2000). Lecticans: organizers of the brain extracellular matrix. Cell. Mol. Life Sci. *57*, 276–289.

Yuan, F., Fang, K.-H., Cao, S.-Y., Qu, Z.-Y., Li, Q., Krencik, R., Xu, M., Bhattacharyya, A., Su, Y.-W., Zhu, D.-Y., et al. (2016). Efficient generation of region-specific forebrain neurons from human pluripotent stem cells under highly defined condition. Sci. Rep. *5*, 18550.

Zamanian, J.L., Xu, L., Foo, L.C., Nouri, N., Zhou, L., Giffard, R.G., and Barres, B.A. (2012). Genomic analysis of reactive astrogliosis. J. Neurosci. *32*, 6391–6410.

Zhang, J., and Herrup, K. (2011). Nucleocytoplasmic Cdk5 is involved in neuronal cell cycle and death in post-mitotic neurons. Cell Cycle *10*, 1208–1214.

Stem Cell Reports, Volume *11*

Supplemental Information

Recapitulation of Human Neural Microenvironment Signatures in iPSC-Derived NPC 3D Differentiation

Daniel Simão, Marta M. Silva, Ana P. Terrasso, Francisca Arez, Marcos F.Q. Sousa, Narges Z. Mehrjardi, Tomo Šarić, Patrícia Gomes-Alves, Nuno Raimundo, Paula M. Alves, and Catarina Brito

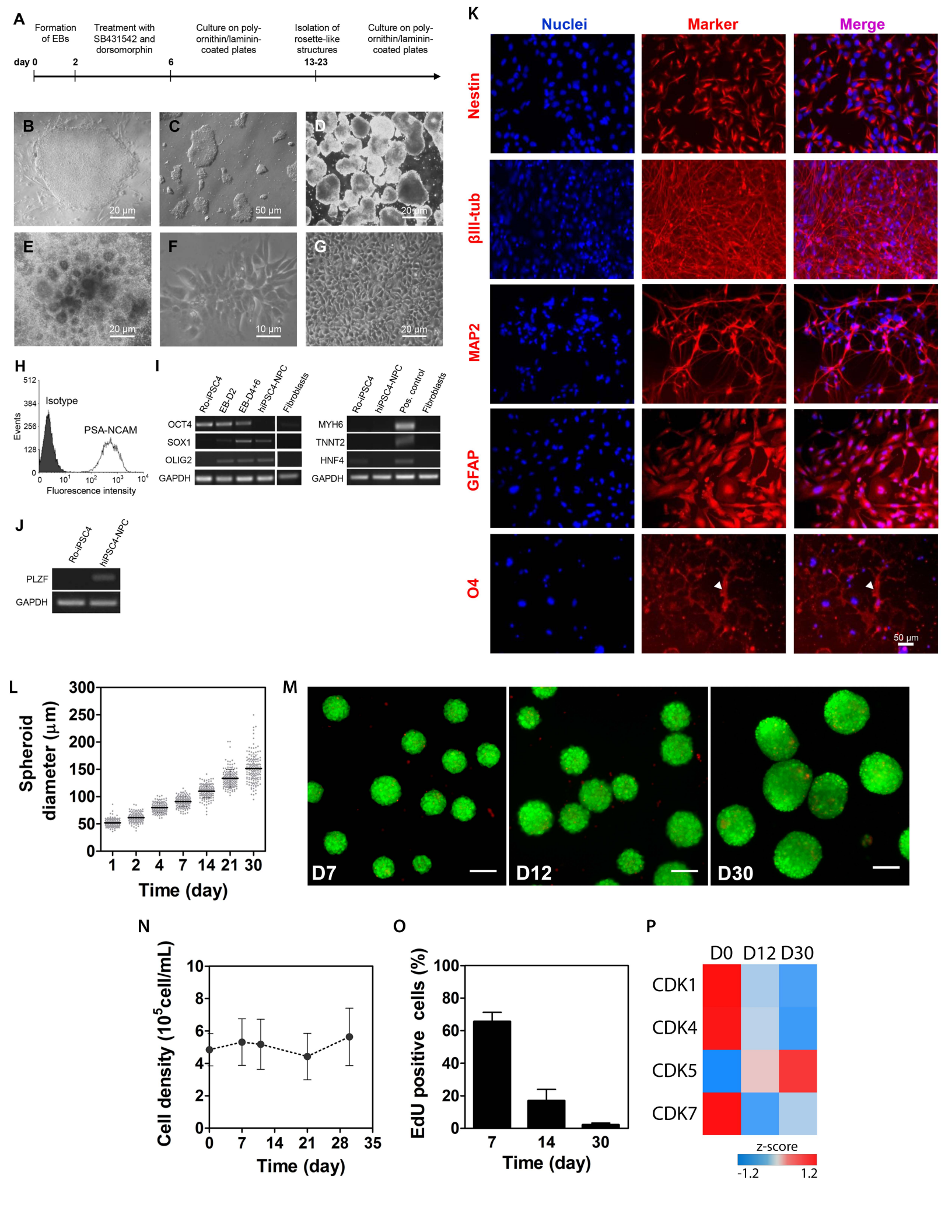
A
Formation of EBs
Treatment with SB431542 and dorsomorphin
Culture on poly-ornithin/laminin-coated plates
Isolation of rosette-like structures
Culture on poly-ornithin/laminin-coated plates
day 0
2
6
13-23
B
C
D
E
F
G
20 μm
50 μm
10 μm
H
Isotype
PSA-NCAM
Events
Fluorescence intensity
I
Ro-iPSC4
EB-D2
EB-D4+6
hiPSC4-NPC
Fibroblasts
Pos. control
OCT4
SOX1
OLIG2
MYH6
TNNT2
HNF4
GAPDH
J
PLZF
K
Nuclei
Marker
Merge
Nestin
βIII-tub
MAP2
GFAP
O4
50 μm
L
Spheroid diameter (μm)
Time (day)
M
D7
D12
D30
N
Cell density (10^5cell/mL)
Time (day)
O
EdU positive cells (%)
Time (day)
P
D0
D12
D30
CDK1
CDK4
CDK5
CDK7
z-score
-1.2
1.2

Figure S1 – Characterization of hiPSC-NPC generation, aggregation and differentiation, related to Figure 1 and Figure 2. (A) Schematic diagram for neural differentiation of hiPSCs. **(B)** R1-hiPSC4 colony grown on MEF feeders (passage 50) and **(C)** after being adapted to grow on Matrigel (passage 55). **(D)** EBs formed by R1-hiPSC4 after collagenase IV treatment cultured in mTesR1 medium for 24 hours. **(E)** Rosette-like structures formed after plating of EBs on PLOL-coated plates for 7-10 days. **(F)** Neuroectodermal cells obtained after plating the dissociated rosette-like structures. **(G)** Confluent monolayer of hiPSC-derived NPCs at passage 10. **(H)** Flow cytometry analysis showing expression of PSA-NCAM on more than 97% of NPCs (passage 10). **(I)** Gene expression of indicated transcripts in undifferentiated R1-hiPSC4, day 2 EBs (EB-d2), day 4-6 EBs (EB-d4-6) and established hiPSC-NPC line as demonstrated by semi-quantitative RT-PCR and agarose gel electrophoresis of PCR products, which were visualized by ethidium bromide staining. Human dermal fibroblasts were used as negative control. hiPSC-NPCs do not express mesodermal markers MYH6 and TNNT2 (expressed in hiPSC-derived cardiomyocytes positive control) and the endodermal marker HNF4-α (expressed in hepatocytes differentiated from hESC line H9 as positive control). **(J)** Gene expression analysis demonstrating that hiPSC-NPCs express PLZF, a marker of early-derived rosette-type neural stem cells, at passage 19. **(K)** Immunocytochemical analysis of R1-hiPSC4-derived NPC demonstrating their neural progenitor identity with the expression of nestin. hiPSC-NPCs cultured for 30 days in neuronal lineage-specific differentiation medium gave rise to neurons expressing pan-neuronal markers βIII-tubulin and MAP2. hiPSC-NPCs differentiate into astrocytes when cultured for 10 days in medium promoting astrocyte differentiation as demonstrated by GFAP staining. Rare O4-positive oligodendrocyte (arrowhead) derived from hiPSC-NPCs after culture in oligodendrocyte-specific medium for 21 days. **(L)** Neurospheroid diameter distribution as a function of time. **(M)** Neurospheroid viability assay, where live cells are stained with fluorescein diacetate (FDA; green) and non-viable cells are labeled with propidium iodide (PI; red). Scale bars, 100 μm. **(N)** Cell density along culture time, evaluated by DNA quantification. Data is presented as mean ± s.e.m. **(O)** Percentage of actively proliferating cells in culture along culture time, assessed by incorporation of EdU. **(P)** Heatmap of cyclin-dependent kinases (CDK) expression levels at D0, D12 and D30. Z-score values were color coded from blue to red, corresponding to downregulation or upregulation, respectively. Data shown represent at least three pooled independent biological experiments (four for panel P, two independent experiments of two cell lines).

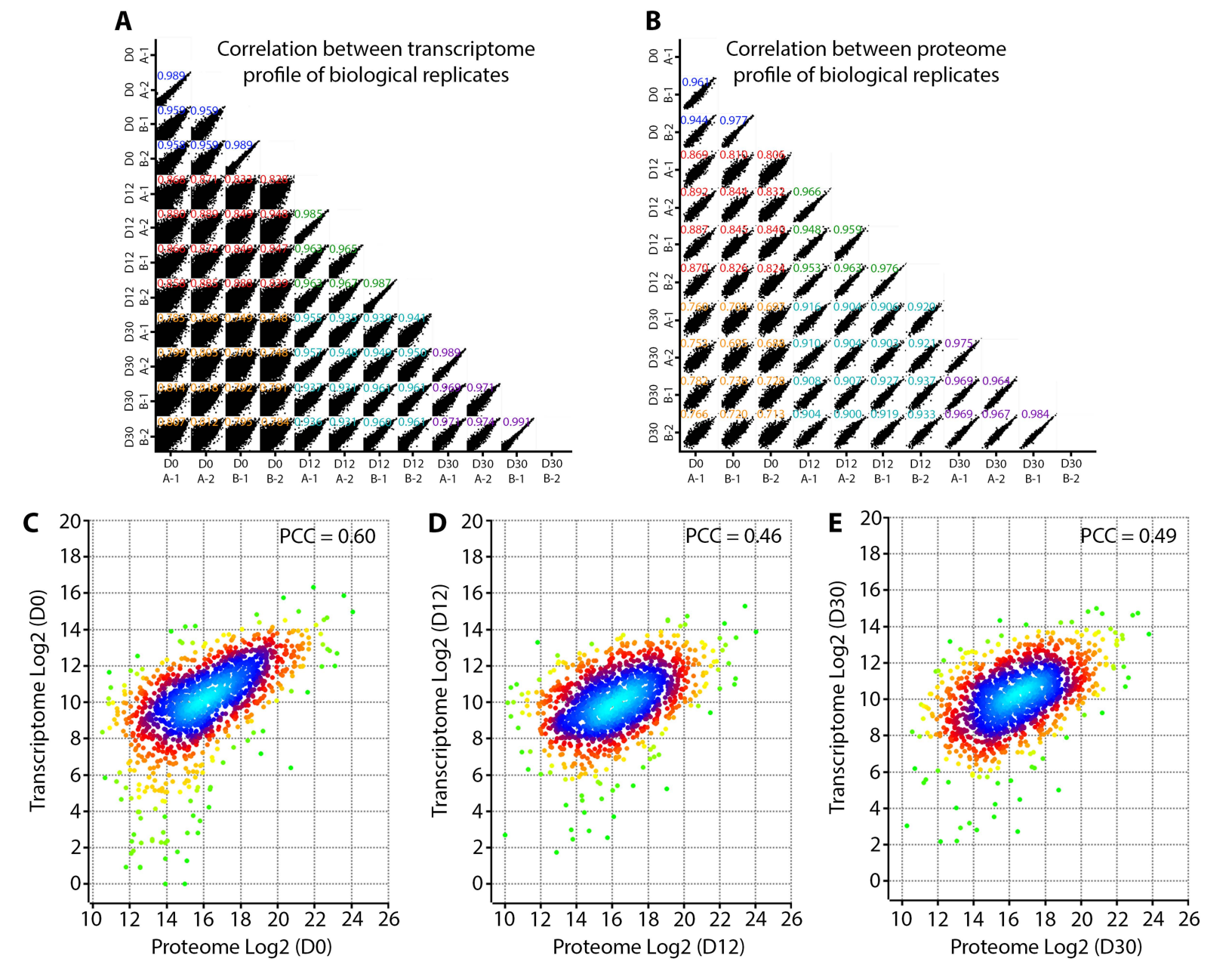
A
Correlation between transcriptome profile of biological replicates
B
Correlation between proteome profile of biological replicates
C
PCC = 0.60
Transcriptome Log2 (D0)
Proteome Log2 (D0)
D
PCC = 0.46
Transcriptome Log2 (D12)
Proteome Log2 (D12)
E
PCC = 0.49
Transcriptome Log2 (D30)
Proteome Log2 (D30)

Figure S2 – Correlation of quantitative data obtained from transcriptome and proteome analyses, related to Figure 1. (A-B) Comparison of the different biological replicates and cell lines (A and B refers to R1-hiPSC1-NPC and R1-hiPSC4-NPC, respectively) at the transcriptome **(A)** and proteome **(B)** level. Each dot represents the quantified levels of a specific transcript/protein. The Pearson correlation coefficients are indicated in each scatterplot. **(C-E)** The density scatterplots describe the correlation obtained for the transcriptome or proteome abundances at day 0 **(C)**, 12 **(D)** and 30 **(E)** of 3D differentiation. Each dot represents the quantified levels of a specific transcript/protein. The Pearson correlation coefficient (PCC) is indicated in the scatterplot. The color code represents the density of dots included in a region of the scatterplot, ranging from high density in blue to low density in green. Data shown represent four pooled independent biological experiments (two independent experiments of two cell lines).

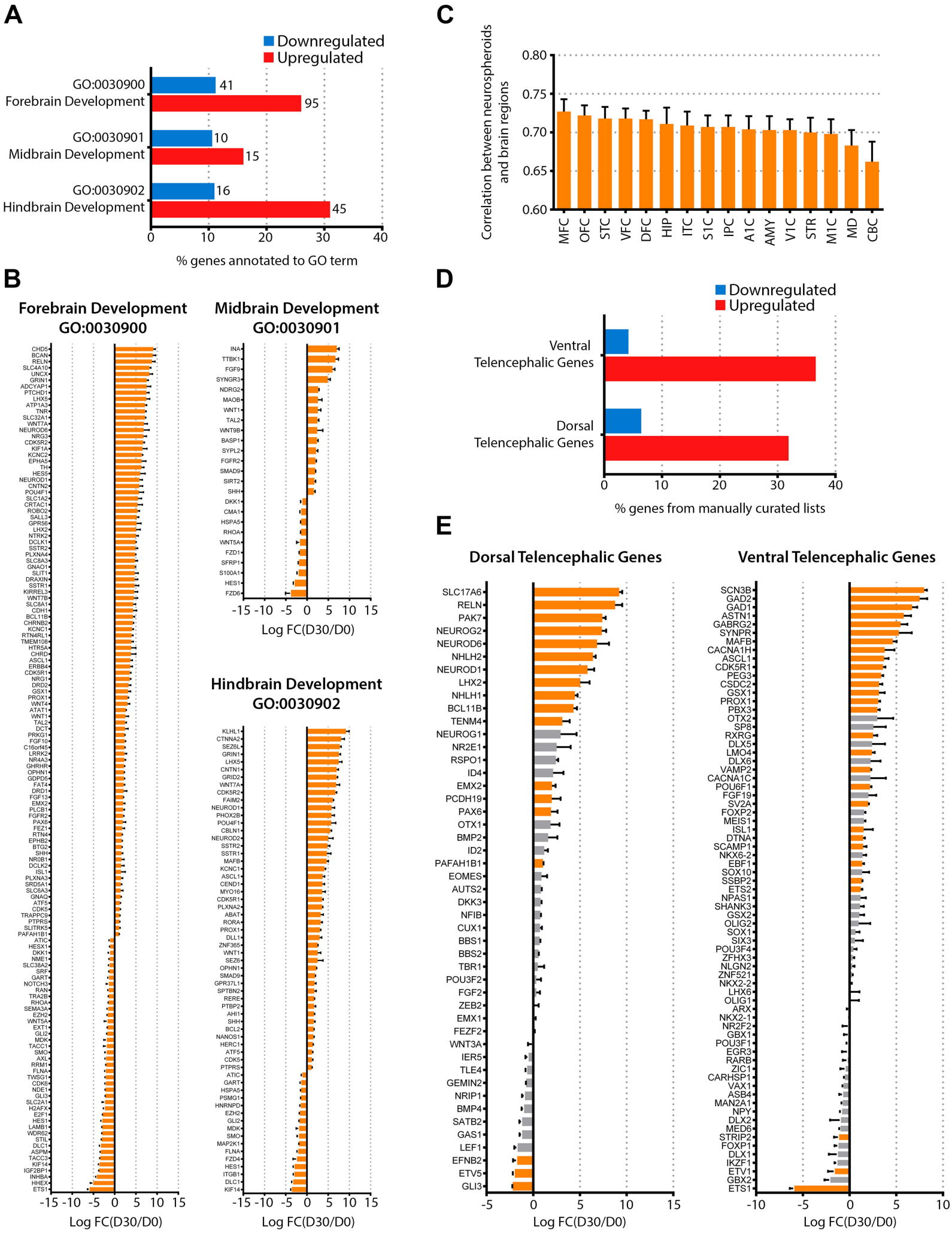
A
Downregulated
Upregulated
GO:0030900
Forebrain Development
41
95
GO:0030901
Midbrain Development
10
15
GO:0030902
Hindbrain Development
16
45
0
10
20
30
40
% genes annotated to GO term
B
Forebrain Development
GO:0030900
Midbrain Development
GO:0030901
Hindbrain Development
GO:0030902
-15 -10 -5 0 5 10 15
Log FC(D30/D0)
C
Correlation between neurospheroids and brain regions
0.80
0.75
0.70
0.65
0.60
MFC
OFC
STC
VFC
DFC
HIP
ITC
S1C
IPC
A1C
AMY
V1C
STR
M1C
MD
CBC
D
Downregulated
Upregulated
Ventral Telencephalic Genes
Dorsal Telencephalic Genes
0
10
20
30
40
% genes from manually curated lists
E
Dorsal Telencephalic Genes
SLC17A6
RELN
PAK7
NEUROG2
NEUROD6
NHLH2
NEUROD1
LHX2
NHLH1
BCL11B
TENM4
NEUROG1
NR2E1
RSPO1
ID4
EMX2
PCDH19
PAX6
OTX1
BMP2
ID2
PAFAH1B1
EOMES
AUTS2
DKK3
NFIB
CUX1
BBS1
BBS2
TBR1
POU3F2
FGF2
ZEB2
EMX1
FEZF2
WNT3A
IER5
TLE4
GEMIN2
NRIP1
BMP4
SATB2
GAS1
LEF1
EFNB2
ETV5
GLI3
-5 0 5 10 15
Log FC(D30/D0)
Ventral Telencephalic Genes
SCN3B
GAD2
GAD1
ASTN1
GABRG2
SYNPR
MAFB
CACNA1H
ASCL1
CDK5R1
PEG3
CSDC2
GSX1
PROX1
PBX3
OTX2
SP8
RXRG
DLX5
LMO4
DLX6
VAMP2
CACNA1C
POU6F1
FGF19
SV2A
FOXP2
MEIS1
ISL1
DTNA
SCAMP1
NKX6-2
EBF1
SOX10
SSBP2
ETS2
NPAS1
SHANK3
GSX2
OLIG2
SOX1
SIX3
POU3F4
ZFHX3
NLGN2
ZNF521
NKX2-2
LHX6
OLIG1
ARX
NKX2-1
NR2F2
GBX1
POU3F1
EGR3
RARB
ZIC1
CARHSP1
VAX1
ASB4
MAN2A1
NPY
DLX2
MED6
STRIP2
FOXP1
DLX1
IKZF1
ETV1
GBX2
ETS1
-10 -5 0 5 10
Log FC(D30/D0)

Figure S3 – Regional specification analysis of differentiated neurospheroids, related to Figure 2. (A) Expression profile summary of genes annotated to the gene ontology (GO) terms for forebrain, midbrain and hindbrain development (365, 94 and 145 genes, respectively). Data are presented as percentage of upregulated (red) or downregulated (blue) genes that are annotated to each GO term, between day 0 and day 30. The number of modulated genes is presented on top of each bar. **(B)** Transcript levels of the genes found to be modulated for each GO term. Data is presented as mean ± s.e.m. of the Log2 fold change between day 0 and 30. **(C)** Correlation analysis between the expression profile of neurospheroids at day 30 and human brain tissue samples from BrainSpan Developmental Transcriptome Dataset. Data is presented as mean ± s.e.m. of correlation coefficient. MFC – anterior (rostral) cingulate (medial prefrontal) cortex; OFC – orbital frontal cortex; STC – posterior (caudal) superior temporal cortex; VFC – ventrolateral prefrontal cortex; DFC – dorsolateral prefrontal cortex; HIP – hippocampus; ITC – inferolateral temporal cortex; S1C – primary somatosensory cortex; IPC – posteroventral (inferior) parietal cortex; A1C – primary auditory cortex; AMY – amygdaloid complex; V1C – primary visual cortex (striate cortex); STR – striatum; M1C – primary motor cortex; MD – mediodorsal nucleus of thalamus; CBC – cerebellar cortex. **(D)** Expression profile summary of dorsal and verntral telencephalic genes. Gene lists were manually curated based on previous publication (Mariani et al., 2012). Data are presented as percentage of upregulated (red) or downregulated (blue) genes, between day 0 and day 30. **(E)** Transcript levels of the dorsal and telencephalic genes. Significantly modulated genes ($p<0.05$ and fold change ±2) are colored orange and non-modulated genes are gray. Data is presented as mean ± s.e.m. of the Log2 fold change between day 0 and 30. Data shown was obtained from four pooled independent biological experiments (two independent experiments of two cell lines).

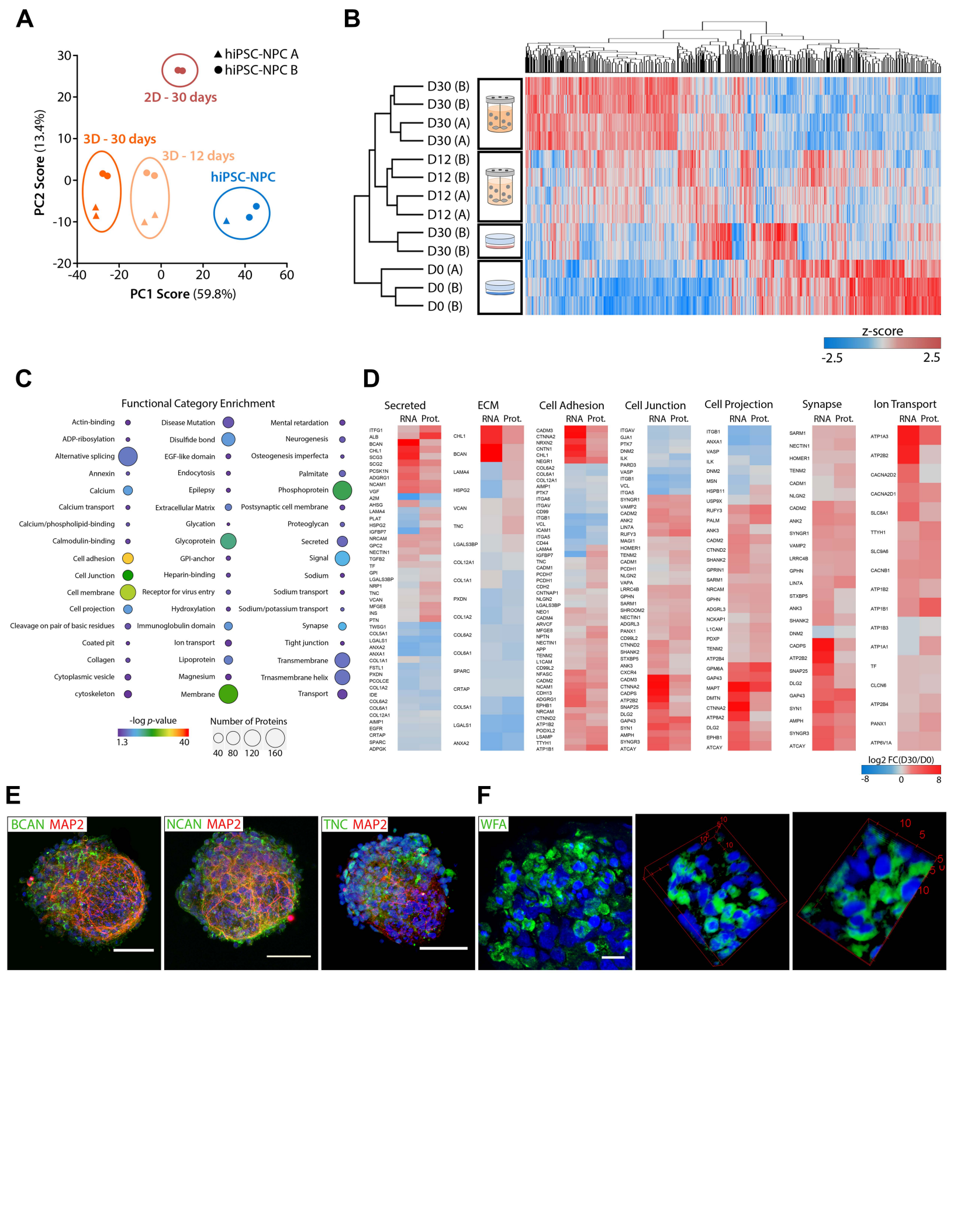
A
▲ hiPSC-NPC A
● hiPSC-NPC B
2D - 30 days
3D - 30 days
3D - 12 days
hiPSC-NPC
PC2 Score (13.4%)
PC1 Score (59.8%)
B
D30 (B)
D30 (B)
D30 (A)
D30 (A)
D12 (B)
D12 (B)
D12 (A)
D12 (A)
D30 (B)
D30 (B)
D0 (A)
D0 (B)
D0 (B)
z-score
-2.5
2.5
C
Functional Category Enrichment
Actin-binding
ADP-ribosylation
Alternative splicing
Annexin
Calcium
Calcium transport
Calcium/phospholipid-binding
Calmodulin-binding
Cell adhesion
Cell Junction
Cell membrane
Cell projection
Cleavage on pair of basic residues
Coated pit
Collagen
Cytoplasmic vesicle
cytoskeleton
Disease Mutation
Disulfide bond
EGF-like domain
Endocytosis
Epilepsy
Extracellular Matrix
Glycation
Glycoprotein
GPI-anchor
Heparin-binding
Receptor for virus entry
Hydroxylation
Immunoglobulin domain
Ion transport
Lipoprotein
Magnesium
Membrane
Mental retardation
Neurogenesis
Osteogenesis imperfecta
Palmitate
Phosphoprotein
Postsynaptic cell membrane
Proteoglycan
Secreted
Signal
Sodium
Sodium transport
Sodium/potassium transport
Synapse
Tight junction
Transmembrane
Trnasmembrane helix
Transport
-log p-value
1.3
40
Number of Proteins
40 80 120 160
D
Secreted
RNA Prot.
ITFG1
ALB
BCAN
CHL1
SCG3
SCG2
PCSK1N
ADGRG1
NCAM1
VGF
A2M
AHSG
LAMA4
PLAT
HSPG2
IGFBP7
NRCAM
GPC2
NECTIN1
TGFB2
TF
GPI
LGALS3BP
NRP1
TNC
VCAN
MFGE8
INS
PTN
TWSG1
COL5A1
LGALS1
ANXA2
ANXA1
COL1A1
FSTL1
PXDN
PCOLCE
COL1A2
IDE
COL6A2
COL6A1
COL12A1
AIMP1
EGFR
CRTAP
SPARC
ADPGK
ECM
RNA Prot.
CHL1
BCAN
LAMA4
HSPG2
VCAN
TNC
LGALS3BP
COL12A1
COL1A1
PXDN
COL1A2
COL6A2
COL6A1
SPARC
CRTAP
COL5A1
LGALS1
ANXA2
Cell Adhesion
RNA Prot.
CADM3
CTNNA2
NRXN2
CNTN1
CHL1
NEGR1
COL6A2
COL6A1
COL12A1
AIMP1
PTK7
ITGA6
ITGAV
CD99
ITGB1
VCL
ICAM1
ITGA5
CD44
LAMA4
IGFBP7
TNC
CADM1
PCDH7
PCDH1
CDH2
CNTNAP1
NLGN2
LGALS3BP
NEO1
CADM4
ARVCF
MFGE8
NPTN
NECTIN1
APP
TENM2
L1CAM
CD99L2
NFASC
CADM2
NCAM1
CDH13
ADGRG1
EPHB1
NRCAM
CTNND2
ATP1B2
PODXL2
LSAMP
TTYH1
ATP1B1
Cell Junction
RNA Prot.
ITGAV
GJA1
PTK7
DNM2
ILK
PARD3
VASP
ITGB1
VCL
ITGA5
SYNGR1
VAMP2
CADM2
ANK2
LIN7A
RUFY3
MAGI1
HOMER1
TENM2
CADM1
PCDH1
NLGN2
VAPA
LRRC4B
GPHN
SARM1
SHROOM2
NECTIN1
ADGRL3
PANX1
CD99L2
CTNND2
SHANK2
STXBP5
ANK3
CXCR4
CADM3
CTNNA2
CADPS
ATP2B2
SNAP25
DLG2
GAP43
SYN1
AMPH
SYNGR3
ATCAY
Cell Projection
RNA Prot.
ITGB1
ANXA1
VASP
ILK
DNM2
MSN
HSPB11
USP9X
RUFY3
PALM
ANK3
CADM2
CTNND2
SHANK2
GPRIN1
SARM1
NRCAM
GPHN
ADGRL3
NCKAP1
L1CAM
PDXP
TENM2
ATP2B4
GPM6A
GAP43
MAPT
DMTN
CTNNA2
ATP8A2
DLG2
EPHB1
ATCAY
Synapse
RNA Prot.
SARM1
NECTIN1
HOMER1
TENM2
CADM1
NLGN2
CADM2
ANK2
SYNGR1
VAMP2
LRRC4B
GPHN
LIN7A
STXBP5
ANK3
SHANK2
DNM2
CADPS
ATP2B2
SNAP25
DLG2
GAP43
SYN1
AMPH
SYNGR3
ATCAY
Ion Transport
RNA Prot.
ATP1A3
ATP2B2
CACNA2D2
CACNA2D1
SLC8A1
TTYH1
SLC9A6
CACNB1
ATP1B2
ATP1B1
ATP1B3
ATP1A1
TF
CLCN6
ATP2B4
PANX1
ATP6V1A
log2 FC(D30/D0)
-8
0
8
E
BCAN MAP2
NCAN MAP2
TNC MAP2
F
WFA

Figure S4 – Proteome remodeling during hiPSC-NPC differentiation, related to Figure 3. (A) Principal component analysis of SWATH-MS data demonstrating a clear clustering of the different experimental groups. **(B)** Heatmap of the proteins significantly modulated during 3D and 2D differentiation (total of 2079 proteins). Hierarchical clustering was performed for rows and columns, where rows represent the different biological replicates of each time point and cell line (A and B refers to R1-hiPSC1-NPC and R1-hiPSC4-NPC, respectively), while each column represents one protein. For the identification of significantly modulated proteins, multi-sample ANOVA test with a permutation-based FDR cutoff of 0.05 was applied on the logarithmized intensities. Z-score values were color coded from blue to red, corresponding to downregulation or upregulation, respectively. **(C)** Functional categories significantly overrepresented (Benjamini Hochberg < 0.05) in proteins annotated as extracellular space or plasma membrane components and significantly modulated during 3D differentiation. The *p*-values and number of proteins are graphically represented by different colors and sphere sizes, respectively. **(D)** Heatmaps of the expression profiles at transcript and protein level of selected categories. Logarithmized fold-changes between D0 and D30 were color coded from blue to red, corresponding to downregulation or upregulation, respectively. Data shown represent four pooled independent biological experiments (two independent experiments of two cell lines). **(E)** Confocal imaging of whole-mount immunostaining, demonstrating the accumulation of important neural ECM components, as brevican (BCAN), neurocan (NCAN) and tenascin-C (TNC). MAP2-positive neuronal cells were also labelled. Scale bars, 50 μm. **(F)** Confocal imaging of wisteria floribunda agglutinin (WFA) labeling in cryosections and 3D rendering insets, demonstrating the presence of neural ECM proteoglycans. Scale bars, 10 μm.

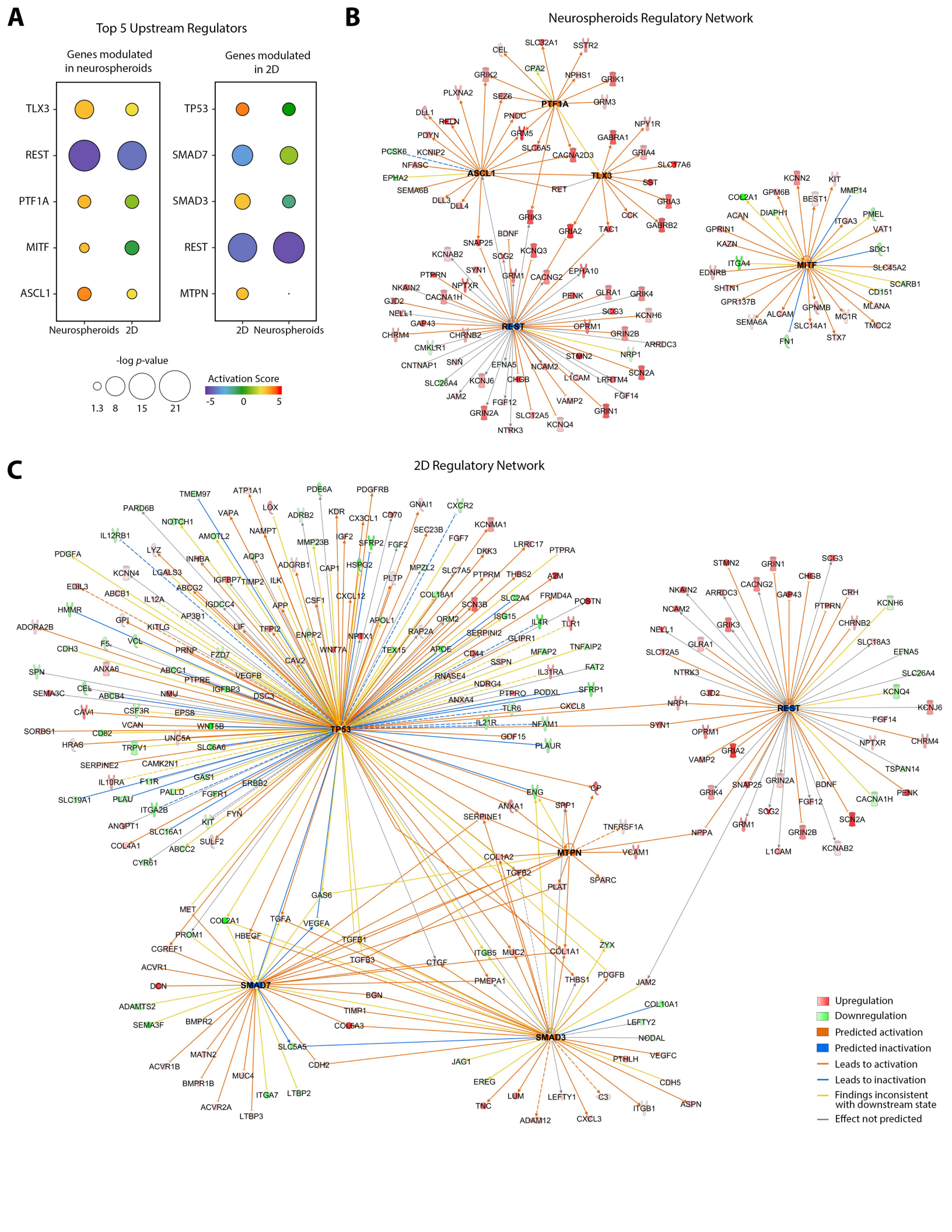
A
Top 5 Upstream Regulators
Genes modulated in neurospheroids
Genes modulated in 2D
TLX3
REST
PTF1A
MITF
ASCL1
TP53
SMAD7
SMAD3
REST
MTPN
Neurospheroids 2D
2D Neurospheroids
-log p-value
1.3 8 15 21
Activation Score
-5 0 5
B
Neurospheroids Regulatory Network
PTF1A
ASCL1
TLX3
REST
MITF
C
2D Regulatory Network
TP53
SMAD7
SMAD3
MTPN
REST
Upregulation
Downregulation
Predicted activation
Predicted inactivation
Leads to activation
Leads to inactivation
Findings inconsistent with downstream state
Effect not predicted

Figure S5 – Upstream regulators analysis for neurospheroids and 2D differentiation, related to Figure 5. (A) Top 5 upstream regulators predicted in Ingenuity Pathway Analysis (IPA) to be responsible for the modulation of all exclusively modulated genes in 3D differentiation (neurospheroids) and 2D differentiation (Srikanth et al., 2015). The activation scores and *p*-values are graphically represented by different colors and sphere sizes, respectively. **(B-C)** Regulatory networks derived for 3D **(B)** and 2D **(C)** data based on IPA predictions for the top 5 upstream regulators.

Supplemental Tables

Table S1 – Two-dimensional annotation enrichment analysis data, indicating the GO-BP terms significantly modulated during 3D differentiation at the transcriptome level and in comparison with the proteome, related to Figure 2

Table S2 – One-dimensional annotation enrichment analysis data, indicating the GO-BP terms significantly modulated in 3D versus 2D differentiation at proteome level, related to Figure 3.

Table S3 – Summary of transcriptome data from the different culture systems, related to Figure 4.

Supplemental Experimental Procedures

Human induced pluripotent stem cells (hiPSC) culture

Human iPSCs (Royan iPSC clone 1 (R1-hiPSC1) and clone 4 (R1-hiPSC4), also known as RIi001-A and RIi007-A, respectively) were derived from dermal fibroblasts as described previously (Totonchi et al., 2010). hiPSC were expanded on Growth Factor Reduced Matrigel Matrix (BD Biosciences) in mTeSR1 medium (StemCell Technologies) under feeder-free culture conditions. Complete medium exchange was performed every day. Cells were maintained under humidified atmosphere with 5 % CO_2, at 37 °C.

Generation and expansion of hiPSC-derived neural progenitor cells (hiPSC-NPC)

hiPSC were detached by treatment with 2 mg/ml of type IV collagenase (Life Technologies) for 15 min at 37°C followed by formation of embryoid bodies (EB) in mTeSR1 medium for 2 days (Figure S1). EBs were treated with 10 µM of SB431542 (TGF-β/Activin/Nodal pathway inhibitor; Selleckchem) and 5 µM dorsomophin (bone morphogenetic protein signaling inhibitor; Sigma-Aldrich) in mTeSR1 for 4 days. On day 6, EBs were plated on previously prepared poly-L-ornithine-laminin (PLOL)-coated surfaces. PLOL coating was prepared by performing a 3 hour incubation at 37°C with 0.16 mg/mL solution of poly-L-ornithine in PBS (with Ca^{2+} and Mg^{2+}), followed by a washing step and a 3 hour incubation at 37°C with 1 µg/mL solution of laminin in PBS (with Ca^{2+} and Mg^{2+}). Cells were then maintained for 7-10 days in DMEM/F12 media with Glutamax (Life Technologies) supplemented with 1% N2 supplement (Life Technologies), 0.1% B27 supplement (Life Technologies), 1.6 µg/mL glucose (Sigma-Aldrich), 20 µg/mL insulin (Sigma-Aldrich), 20 ng/mL rhu-bFGF (Peprotech) (Koch et al., 2009). To establish NPC lines, differentiated EBs were treated with 0.1 mg/ml dispase (Life Technologies) for 15 min at 37°C to isolate the rosette structures from the surrounding flat cells. Isolated cell clusters were then washed once with PBS without Ca^{2+} and Mg^{2+} and treated with 1 mg/ml collagenase IV for 5 min at 37°C. After removing the enzyme, loose clusters were washed once with PBS without Ca^{2+} and Mg^{2+} and dissociated with 0.05% trypsin-EDTA (Life Technologies) for 3 min. Cells were then plated on PLOL-coated surfaces in the NPC expansion medium, composed of DMEM/F12 media with Glutamax (Life Technologies) supplemented with 1% N2 supplement (Life Technologies), 0.1% B27 supplement (Life Technologies), 1.6 µg/mL glucose (Sigma-Aldrich), 20 µg/mL insulin (Sigma-Aldrich), 20 ng/mL rhu-bFGF (Peprotech) and 20 ng/ml rhu-EGF (Sigma-Aldrich). Medium was changed every other day until confluent cell culture was obtained. For further expansion and maintenance hiPSC-NPC were split typically every 4-5 days at 90-100% confluence. Cells were dislodged through incubation with 0.05% Trypsin-EDTA for 1-2 minutes, ressuspended in DMEM supplemented with 10% FBS (Life Technologies), sedimented by centrifugation and the resultant pellet ressuspended in NPC expansion medium. Cell concentration and viability were determined by the trypan blue exclusion method in a Fuchs-Rusenthal hemocytometer. The cell suspension was used to inoculate PLOL-coated T-flasks, at a cell density of 3 x 10^4 cell/cm^2. A 50 % media exchange was performed at day 2 of culture. Cells were maintained under humidified atmosphere, in a multi-gas cell incubator (Sanyo), with 5 % CO_2 and 3 % O_2, at 37 °C.

hiPSC-NPC lineage-specific 2D differentiation

To differentiate hiPSC-NPC to neuronal cells, 1x10^4 cells/cm^2 were plated on PLOL-coated plates in the NPC expansion medium. Next day, medium was changed to DMEM/F12 supplemented with neurobasal medium (1:1; Life Technologies), 1% N-2 Supplement, 1% B-27 Supplement, 200 µM ascorbic acid (Wako, Neuss, Germany) and cells cultured for 2 weeks. Half of the medium was replaced every other day. After 2 weeks of culture, the ratio of neurobasal to DMEM/F12 medium was changed to 3:1, N-2 Supplement was reduced to 0.5% and 10 ng/ml BDNF of brain derived neurotrophic factor (BDNF; R&D, Wiesbaden-Nordenstadt, Germany) was added and cells cultured for one additional week. Half of the medium was changed every other day. To differentiate hiPSC-NPC to astrocytes, 5x10^4 cells/cm^2 were plated on PLOL-coated plate. After 24 hours, medium was changed to DMEM/F12 containing 10% FBS, 1% minimum essential medium NEAA (MEM-NEAA) and 1% L-glutamine (all from Life Technologies) for 7-10 days. 75% of medium was changed every other day. For differentiation of hiPSC-NPC to oligodendrocytes, 5x10^4 cells/cm^2 were plated on PLOL-coated plate in the NPC expansion medium. Next day, half of the medium was changed to DMEM/F12 medium supplemented with 2% B-27 Supplement, 2 mM L-glutamine, 10 µg/ml insulin, 10 µg/ml putrescine, 63 ng/ml progesterone, 50 ng/ml sodium selenite, 40 ng/ml triiodothyronine (T3), 50 µg/ml holo-transferrin and 20

ng/ml EGF (all from Sigma-Aldrich). After one week, the cells were dissociated with 0.05% trypsin–EDTA, $1.5x10^4$ cells/cm^2 were plated on PLOL- coated plates and further cultured for 2 weeks. Medium was changed every other day.

hiPSC-NPC 3D and 2D differentiation

hiPSC-NPC were expanded and dislodged with trypsin into a cell suspension, as described above. This cell suspension was passed through a 70 µm nylon strainer (Millipore) prior to bioreactor inoculation, in order to eliminate cell clumps. The obtained single cell suspension was diluted for a cell density of $4x10^5$ cell/mL in aggregation medium (AM), with the same composition as EM, except for reduced EGF/FGF concentration (5 ng/mL) and the addition of 5 µM Y-27632. Cells were then inoculated into software-controlled stirred-tank DASGIP® Bioblock bioreactor system (Eppendorf), as described previously (Simão et al., 2016). Culture conditions were set to maintain cells under 3 % dissolved oxygen (15 % of air with 21 % of oxygen), pH 7.4, 37 ºC and a stirring rate of 70 rpm. In order to control the aggregate size and avoid aggregate fusion, the stirring rate was gradually increased up to 90 rpm with 10 rpm steps, based on visual inspection of the culture. After 48 hours of culture, perfusion operation mode was activated, with a dilution rate of 0.33 day^{-1} (i.e., 33 % working volume exchange *per* day) under gravimetric control. To prevent the loss of aggregates through the outlet perfusion line, a metallic filter of 20 µm pore size was adopted as cell retention device (Simão et al., 2016). After a 7 day aggregation period with AM, differentiation was induced by replacing the perfusion medium with differentiation medium (DM), maintain the culture for further 23 days (total of 30 days). DM was prepared by supplementing DMEM/F12 with Glutamax with 2 % B27 supplement, 1.6 µg/mL glucose, 10 µg/mL insulin, 10 µg/mL putrescin, 63 ng/mL progesterone, 50 µg/mL apotransferrin, 50 ng/mL sodium selenium (all from Sigma-Aldrich) and 200 mM ascorbic acid (Wako). For 2D differentiation, cells were plated in PLOL-coated surfaces at a cell density of 3×10^4 cell/cm^2 in EM. On the day after culture medium was changed to DM and every other day half of the medium was exchanged to fresh DM. At day 7, cells were dislodged by incubating with 0.05% Trypsin-EDTA for 1-2 minutes and replated on PLOL-coated surfaces at a cell density of 5×10^4 cell/cm^2 in DM. Cells were then further cultured for 23 days (total of 30 days), where half of the medium was exchanged to fresh DM every other day.

Immunofluorescence microscopy

Cells were fixed in 4% paraformaldehyde + 4% sucrose in phosphate-buffered saline (PBS) for 20 min at room temperature and washed three times with PBS. For cryosectioning samples were dehydrated with 30% (w/v) sucrose overnight, frozen at -80 ºC in Tissue-Tek O.C.T. (Sakura) and sectioned at a thickness of 10 mm using a cryomicrotome (Cryostat I, Leica). For immunofluorescence, cells were permeabilized with 0.5 M ammonium chloride and 0.25% Triton X-100 in PBS (Figure S1K) or with 0.1% TritonX-100 in PBS (Figures 2C, 3F and S1P). Cells were blocked for 1 hour with 5% goat or rabbit serum in PBS (Figure S1K) or for 30 min with 0.2% fish skin gelatin in PBS (Figures 2C, 3F). Primary antibodies were then incubated overnight at 4°C diluted in 0.8% bovine serum albumin (BSA) in PBS (Figure S1K) or for 2 hours diluted in 0.1% TritonX-100 + 0.125% fish skin gelatin in PBS (Figures 2C, 3F). Cells were washed three times with PBS and incubated for 1 hour with secondary antibodies diluted in 0.8% BSA in PBS (Figure S1K) or 0.125% fish skin gelatin in PBS (Figures 2C, 3F). Primary and secondary antibodies were used as follows: anti-nestin (AB5922, Millipore), anti-Sox2 (AB5603, Millipore), anti-βIII-tubulin (1:200, MAB1637, Millipore; or 1:1000, sc-80005, Santa Cruz), anti-synaptophysin (1:200, MAB5258, Millipore), anti-MAP2 (1:10 000, ab5392, Abcam; or 1:500, sc-20172, Santa Cruz), anti-GFAP (1:200, AB5804, Millipore; or 1:500, G3893, Sigma-Aldrich), anti-O4 (1:500, O7139, Sigma-Aldrich), AlexaFluor 488 goat anti-mouse IgG, AlexaFluor 594 goat anti-chicken IgY or AlexaFluor 594 goat anti-rabbit IgG, AlexaFluor 488 goat anti-rabbit IgG (1:500; all from Life Technologies). Cell nuclei were counterstained with Hoechst, DAPI or TO-PRO-3 (Life Technologies). Coverslips were mounted in ProLong Gold antifade reagent with DAPI (Life Technologies). Preparations were visualized on an Axiovert 200M fluorescence microscope (Carl-Zeiss) or point-scan confocal microscope (SP5, Leica). The obtained images were processed using FIJI software (Schindelin et al., 2012) and only linear manipulations were performed.

Flow cytometry

Single-cell suspensions of hiPSC-NPC were prepared by 0.05% trypsin-EDTA treatment as described above. The dissociated cells were centrifuged, washed and filtered through a 40 µm cell strainer (BD Pharmingen). Cell density was determined and cells were resuspended in the appropriate

volume of staining buffer (PBS supplemented with 0.1% FBS) to obtain a cell density of 0.5 $x10^6$ cells/50 µl. Cells were then dispensed into 1.5 ml microcentrifuge tubes (50 µl/tube) and stained either with isotype control or antigen-specific PSA-NCAM antibody (1:100, MAB5324, Millipore), followed by 30 minutes incubation with AlexaFluor 555 secondary antibody (dilution 1:1000). The cells were washed two times with staining buffer and data collected on the flow cytometer (Attune® Acoustic Focusing Cytometer, Thermo Fisher Scientific). Cells were gated on forward and side scatter dot plots. 10,000 events per sample were acquired and the data were analyzed with Attune software.

Viability assay

For cell viability assessment, neurospheres were incubated with 20 mg/mL fluorescein diacetate, which stains viable cells, and 10mg/mL propidium iodide, a membrane-impermeable DNA dye that stains nonviable cells in PBS for 5 min, washed with PBS, and observed using fluorescence microscopy (DMI6000, Leica).

DNA quantification-based cell concentration determination

For cell density determination, 0.5 mL samples were collected, sedimented by centrifugation at 1000 x g, 5 min and resuspended in ultrapure distilled water. Complete cell lysis was achieved through a freeze-thaw cycle in liquid nitrogen coupled to 15 min sonication into an ultrasound bath at 35 kHz. DNA quantification was performed using the Quant-iT™ PicoGreen® dsDNA Assay Kit (Life Technologies), according to the manufacturer's instructions. Fluorescence intensity was measured in spectrofluorometer at 480 nm excitation and 520 nm emission wavelengths. The obtained values were correlated with calibration curves performed by serial dilutions of standard DNA solutions and cell lysates from samples with known cell concentrations.

Aggregate Size Determination

Neural spheroid size determination was performed by imaging analysis of phase contrast images, using the open source FIJI software (Schindelin et al., 2012). Briefly, the aggregate boundaries were defined by manual threshold adjustment and the Feret's diameter was automatically determined for each one of the neurospheres.

Cell proliferation Assessment

The percentage of proliferative cells within neurospheres was determined through the EdU (5-ethynyl-2´-deoxyuridine) incorporation assay, using the Click-iT® EdU Alexa Fluor® 488 Assay Kit (Life Technologies). Briefly, neurospheres were allowed to adhere to PLOL-coated glass coverslips and incubated with 10 µM EdU in culture media for 20 h. After incubation, cells were fixed with 4 % paraformaldehyde (PFA) and 4 % sucrose in PBS for 20 min, washed twice with PBS with 1 % bovine serum albumin (BSA) and permeabilized with saponin-based working reagent for 20 to 30 min, depending on neural spheroid size. Cells were incubated with AlexaFluor488 anti-EdU antibody, according to manufacturer's instructions, for 45 min to 1 h 15 min, depending on neural spheroid size. Coverslips were mounted in ProLong Gold antifade reagent with DAPI (Life Technologies). Preparations were visualized in spinning disk microscope (Nikon Eclipse Ti-E, confocal scanner: Yokogawa CSUx1) and resultant images processed in FIJI software. For quantitative analysis, Edu-positive cells and total DAPI-labeled nuclei were determined using cell counter plug-in in FIJI (Schindelin et al., 2012).

RT-PCR

Total RNA was isolated from hiPSC, EB and hiPSC-NPC by TRIzol reagent (Life Technologies) following the manufacturer's recommendations. RNA concentration was measured with a Nanodrop 1000 (Thermo Scientific, Frankfurt, Germany) and the quality was assessed by agarose gel electrophoresis. cDNA samples were synthesized from 1 µg of total RNA using the SuperScript II First-Strand Synthesis Kit and random hexamers (Life Technologies) for priming. RT-PCR was carried out using DreamTaq Green PCR Master Mix (Thermo Scientific, Frankfurt, Germany) and PCR products were analyzed by agarose gel electrophoresis with a DNA ladder mix (SM0331, Life Technologies) to determine the PCR product sizes. The following primers were used: OCT4 (fwd 5'-AGGGCAAGCGATCAAGCA-3' and rev 5'-AGGGCAAGCGATCAAGCA-3'); SOX1 (fwd 5'-CAATGCGGGGAGGAGAAGTC-3' and rev 5'-CTCTGGACCAAACTGTGGCG-3'); OLIG2 (fwd 5'-

CAGAAGCGCTGATGGTCATA-3' and rev 5'-TCGGCAGTTTTGGGTTATTC-3'); MYH6 (fwd 5'-TGTCCCGGGAAGGGGGCAAA-3' and rev 5'-CCGGCTCGTGCAGGAAGGTC-3'); TNNT2 (fwd 5'-GGTGCCTCCCAAGATCCCCG-3' and rev 5'-GATGCGCTGCTGCTCGGCCC-3'); HNF4 (fwd 5'-CTGCTCGGAGCCACCAAGAGATC-3' and rev 5'-ATCATCTGCCAGGTGATGCTCTGCA-3'); PLZF (fwd 5'-CTATGGGCGAGAGGAGAGTG-3' and rev 5'-TCAATACAGCGTCAGCCTTG-3'); GAPDH (fwd 5'-GGACTCATGACCACAGTCCAT-3' and rev 5'-ACCTTGCCCACAGCCTTG-3').

Sample preparation for mass spectrometry

Samples from 3D cultures were directly harvested from the bioreactor. 2D differentiated cells were harvested by gentle mechanical dislodgment using a cell scrapper. Cells were then sedimented by centrifugation at 300 x*g*, 5 min. Supernatant was discarded and resulting cell pellet was washed with PBS, followed by centrifugation at 300 x*g*, 5 min. Cells were lysed in Triton X-100 lysis buffer (50 mM Tris, 5 mM EDTA, 150 mM NaCl, 1% Triton X-100 (all from Sigma-Aldrich) and 1x complete protease inhibitors cocktail (Roche)), for 45 minutes at 4ºC. Protein quantification was performed using Micro BCA™ Protein Assay Kit (Thermo Fisher Scientific) following manufacturer's instructions. Proteins were precipitated using methanol, as previously described (Wessel and Flügge, 1984). Briefly, proteins were precipitated in four-fold excess of methanol, centrifuged at 9 000 x*g* for 10 seconds and followed by the addition of 2 parts of chloroform with subsequent centrifugation. For phase separation, 3 parts of deionized water were added to the samples, homogenized by vigorous vortex and centrifuged at 9 000 x*g* for 1 min. The upper phase was discarded and 3 parts of methanol were added. Samples were mixed, and centrifuged at 9 000 x*g* for 2 min to pellet precipitated protein. Supernatant was removed and precipitates were dried by heating at 60 °C with lids slightly ajar. For surfactant assisted in-solution protein digestion, precipitated proteins were solubilized in 0.1% of RapiGest SF Surfactant (Waters). Prior to digestion, samples were reduced with 5 mM of dithiothreitol (DTT) for 30 mins at 60 °C, alkylated with 15 mM iodoacetamide (IAA) for 30 min in dark and boiled at 100 °C for 5 mins. After cooling to room temperature, protein digestion was performed by overnight incubation with trypsin (Promega; 1.2 µg per 100 µg protein) at 37 °C. Trypsin inactivation was achieved by acidification with trifluoroacetic acid (TFA) at 0.5 % and incubation at 37 °C for 45 min. Samples were centrifuged at 16 000 x*g* for 10 min, supernatants were collected into new tubes and dried using a Savant™ Universal SpeedVac™ concentrator (Thermo Fisher Scientific).

Generation of the spectral reference library

Seven samples from different experimental group were used for information-dependent acquisition (IDA) analysis by NanoLC-MS using TripleTOF 6600 (ABSciex, Framingham, MA, USA). A reversed phase nanoLC with a trap and elution configuration, using a Nano cHiPLC Trap column (200 µm × 0.5 mm ChromXP C18-CL 3 µm 120 Å) and nano column (75 µm × 15 cm ChromXP C18-CL 3 µm 120 Å) was performed. Water with 0.1% (v/v) formic acid (solvent A) and acetonitrile with 0.1% (v/v) formic acid (solvent B) were used. Sample was loaded in the trap column at a flow rate of 2 µL.min-1 for 10 min using 100% (v/v) solvent A. Peptide separation was performed in the nano column at a flow rate of 300 $\mu L.min^{-1}$ applying a 90 min linear gradient of 5% to 30% (v/v) of solvent B. Each sample was subjected to two IDA runs. The mass spectrometer was set for IDA scanning full spectra (400–2000 m/z) for 250 ms. The top 50 ions were selected for subsequent MS/MS scans (150–1800 m/z for 40 ms each) using a total cycle time of 2.3 s. The selection criteria for parent ions included a charge state between +2 and +5, and counts above a minimum threshold of 125 counts per second. Ions were excluded from further MS/MS analysis for 12 s. Fragmentation was performed using rolling collision energy with a collision energy spread of 5.

The spectral library was created by combining all IDA raw files using ProteinPilot™ software (v5.0 ABSciex) with the Paragon algorithm and with the following search parameters: search against Homo sapiens from Uniprot/SwissProt database (release 2015_05); trypsin digestion; iodoacetamide cysteine alkylation; through identification efforts. After a false discovery rate (FDR) analysis, only FDR<1% were considered (3272 proteins). The output of these searches, in the form of a group file, was used as the reference spectral library. An extended spectral library was built by merging the spectral library containing the IDA runs with an in-house spectral library of human samples, using SwathXtend R package (Wu and Pascovici, 2015). This spectral ion library contains 5458 proteins.

Quantitative proteomic analysis

For quantitative analysis, 2.5 µg of each sample were subjected to three SWATH runs (Sequential Windowed data independent Acquisitions of the Total High-resolution Mass Spectra). Similar chromatographic conditions to the previously described IDA runs were used. The mass spectrometer was operated in a cyclic product ion data independent acquisition (DIA). A variable windows calculator and SWATH acquisition method editor (AB SCIEX) were used to setup the SWATH acquisition. A set of 32 overlapping windows (containing 1 m/z for the window overlap) was constructed, covering the precursor mass range of 400 – 1200 m/z. A 50 ms survey scan was acquired at the beginning of each cycle, and SWATH MS/MS spectra were collected for 96 ms resulting in a cycle time of 3.172 s. Rolling collision energy with a collision energy spread of 15 was used. The spectral alignment and targeted data extraction of DIA samples were performed using PeakView v.2.1 (AB SCIEX; Framingham, US) with the reference spectral library. For data extraction the following parameters were used: six peptides/protein, six transitions/peptide, peptide confidence level of >99%, FDR threshold of 1%, excluded shared peptides, and extracted ion chromatogram (XIC) window of 10 min and width set at 20 ppm. A total of 3728 proteins were quantified under these conditions. One sample that did not meet quality standards was removed from further analysis (day 0 from cell line R1-hiPSC1-NPC). The mass spectrometry proteomics data have been deposited to the ProteomeXchange Consortium via the PRIDE (Vizcaíno et al., 2016) partner repository with the dataset identifier PXD007130.

Next Generation Sequencing

Total RNA was extracted using the RNeasy Mini Kit (Qiagen), according to the manufacturer's instructions and quantified using a NanoDrop 2000c (Thermo Scientific). The RNA was sequenced using a Illumina HiSeq 4000 instrument at the Transcriptome and Genome Analysis Laboratory of the Universitaetsmedizin Goettingen. The raw sequences were mapped to the Ensembl Human Genome Assembly GRCh38.p10 using StrangNGS software (http://www.strand-ngs.com/). After mapping and counting, the data were normalized using quantile using StrandNGS. The accession number for the RNA sequencing data reported in this paper is NCBI GEO: GSE102139.

Proteome and transcriptome data analysis

Bioinformatic data analysis was performed using Perseus software environment (Tyanova et al., 2016). Statistical analysis of transcriptome and proteome was performed on logarithmized intensities for transcripts/proteins identified in at least one experimental condition. Significantly modulated transcripts/proteins were identified by performing ANOVA or t-test with a permutation-based FDR cutoff of 0.05. Annotation matrix algorithm (Cox and Mann, 2012) was used to identify the gene ontology biological processes (GO-BP) significantly overrepresented in the datasets (Benjamini-Hochberg FDR lower than 0.02 or 0.05, as indicated in figure captions) and correlated these with an expression level score. The identification of GO-BP terms enriched in the top 1000 principal component analysis loadings was performed using DAVID 6.8 (Huang et al., 2009). The pathway analysis, transcription factor activity prediction and transcriptional network analysis were performed using Ingenuity Pathway Analysis (IPA) as described (Murdoch et al., 2016; Raimundo et al., 2012). Datasets of hiPSC-NPC 2D differentiation were downloaded from GSE71289. Datasets containing samples from hPSC, embryoid bodies, cortical organoids and fetal cortex (male, 19 weeks gestation) were downloaded from GSE82022. Batch normalization was performed using ComBat function (Johnson et al., 2007) on Surrogate Variable Analysis R package within R/Bioconductor (Gentleman et al., 2004). BrainSpan Developmental Transcriptome Dataset (publicly accessible via the Allen Brain Atlas data portal - www.brainspan.org) was used for correlation analysis between the transcriptome profile of neurospheroids and human brain tissue samples. Batch normalization was performed using ComBat function in R and correlation coefficients were determined using CORREL function of Microsoft Excel. Each neurospheroid sample at day 30 was compared with each tissue sample and correlation coefficients for the four neurospheroid samples were averaged. Data was then averaged for brain region, excluding regions with less than 20 samples.

Supplemental References

Cox, J., and Mann, M. (2012). 1D and 2D annotation enrichment: a statistical method integrating quantitative proteomics with complementary high-throughput data. BMC Bioinformatics *13*, S12.

Gentleman, R.C., Carey, V.J., Bates, D.M., Bolstad, B., Dettling, M., Dudoit, S., Ellis, B., Gautier, L., Ge, Y., Gentry, J., et al. (2004). Bioconductor: open software development for computational biology and bioinformatics. Genome Biol. *5*, R80.

Huang, D.W., Lempicki, R. a, and Sherman, B.T. (2009). Systematic and integrative analysis of large gene lists using DAVID bioinformatics resources. Nat. Protoc. *4*, 44–57.

Johnson, W.E., Li, C., and Rabinovic, A. (2007). Adjusting batch effects in microarray expression data using empirical Bayes methods. Biostatistics *8*, 118–127.

Koch, P., Opitz, T., Steinbeck, J.A., Ladewig, J., and Brustle, O. (2009). A rosette-type, self-renewing human ES cell-derived neural stem cell with potential for in vitro instruction and synaptic integration. Proc. Natl. Acad. Sci. *106*, 3225–3230.

Mariani, J., Simonini, M.V., Palejev, D., Tomasini, L., Coppola, G., Szekely, A.M., Horvath, T.L., and Vaccarino, F.M. (2012). Modeling human cortical development in vitro using induced pluripotent stem cells. Proc. Natl. Acad. Sci. U. S. A. *109*, 12770–12775.

Murdoch, J.D., Rostosky, C.M., Gowrisankaran, S., Arora, A.S., Soukup, S.-F., Vidal, R., Capece, V., Freytag, S., Fischer, A., Verstreken, P., et al. (2016). Endophilin-A Deficiency Induces the Foxo3a-Fbxo32 Network in the Brain and Causes Dysregulation of Autophagy and the Ubiquitin-Proteasome System. Cell Rep. *17*, 1071–1086.

Raimundo, N., Song, L., Shutt, T.E., McKay, S.E., Cotney, J., Guan, M.X., Gilliland, T.C., Hohuan, D., Santos-Sacchi, J., and Shadel, G.S. (2012). Mitochondrial stress engages E2F1 apoptotic signaling to cause deafness. Cell *148*, 716–726.

Schindelin, J., Arganda-Carreras, I., Frise, E., Kaynig, V., Longair, M., Pietzsch, T., Preibisch, S., Rueden, C., Saalfeld, S., Schmid, B., et al. (2012). Fiji: an open-source platform for biological-image analysis. Nat. Methods *9*, 676–682.

Simão, D., Arez, F., Terasso, A.P., Pinto, C., Sousa, M.F.Q., Brito, C., and Alves, P.M. (2016). Perfusion Stirred-Tank Bioreactors for 3D Differentiation of Human Neural Stem Cells. In Bioreactors in Stem Cell Biology, K. Turksen, ed. (Springer New York), pp. 129–142.

Totonchi, M., Taei, A., Seifinejad, A., Tabebordbar, M., Rassouli, H., Farrokhi, A., Gourabi, H., Aghdami, N., Hosseini-Salekdeh, G., and Baharvand, H. (2010). Feeder- and serum-free establishment and expansion of human induced pluripotent stem cells. Int. J. Dev. Biol. *54*, 877–886.

Tyanova, S., Temu, T., Sinitcyn, P., Carlson, A., Hein, M.Y., Geiger, T., Mann, M., and Cox, J. (2016). The Perseus computational platform for comprehensive analysis of (prote)omics data. Nat. Methods *13*, 731–740.

Vizcaíno, J.A., Csordas, A., Del-Toro, N., Dianes, J.A., Griss, J., Lavidas, I., Mayer, G., Perez-Riverol, Y., Reisinger, F., Ternent, T., et al. (2016). 2016 update of the PRIDE database and its related tools. Nucleic Acids Res. *44*, D447–D456.

Wessel, D., and Flügge, U.I. (1984). A method for the quantitative recovery of protein in dilute solution in the presence of detergents and lipids. Anal. Biochem. *138*, 141–143.

Wu, J., and Pascovici, D. (2015). SwathXtend: SWATH extended library generation and statistical data analysis.